nature immunology

Article

https://doi.org/10.1038/s41590-026-02581-9

Mechanosensing by T cells promotes a tissue-resident memory transcriptional program

Received: 3 October 2025

Accepted: 5 June 2026

Published online: 3 July 2026

Check for updates

Jérémy Postat[1,2,13], Mauricio Merino[2,3,13], Angela R. Mingarelli[1,2,13], Aysha Cerf[2,3], Aanya Bhagrath[1,2], Dhanesh Patel[1,2], Connie Shen[2,3], Johanna Brodbeck[1,2], Pouria Tirgar[4], Dakota Rogers[1,2], Jules Blanc[1,2], Thiviya Jeyakumar[2,5], Caitlin Schneider[2,3], Shana Coley[6], Nadia Giannetti[7,8], Taylor A. DePauw[9], Johannes Textor[10], Allen Ehrlicher[4], Stephen C. Jameson[9], Reza Sharif-Naeini[1,11], Abhinav Sharma[8,12] & Judith N. Mandl[1,2,3]

Cell migration and strategic positioning within tissues is critical for the rapid mobilization of a T cell response. T cells must remain motile in both lymphoid and nonlymphoid tissues, which vary widely in mechanical properties such as stiffness. Here we showed that activated T cells sensed mechanical cues and responded with changes in cell morphology, nuclear envelope composition and initiation of DNA repair to protect their genomic material from force-mediated damage. Increased mechanical input also drove the transcriptional reprogramming of activated T cells, including changes in many of the core genes shared by tissue-resident memory T cells across diverse tissues, by modulating the expression of the tissue-resident memory T cell-associated transcription factors Klf2, Runx3 and Hic1. Thus, mechanosensing by activated T cells impacted T cell fate, promoting a transcriptional program associated with tissue residency.

Immune cell migration and strategic positioning within tissues is critical to the rapid mobilization of an immune response. T cells continuously traffic between and within secondary lymphoid organs to survey for antigen[1]. Upon activation, they are licensed to enter other tissues via chemokine receptor and integrin expression to participate in pathogen clearance. A fraction of effector T cells establish a tissue-resident, noncirculating population of tissue-resident memory (T_{RM}) cells that accelerate protection from reinfection, but can also mediate tissue pathology in transplant rejection or autoimmunity[2,3]. Effector T cells encounter a range of tissue microenvironments that vary in stiffness, confinement and extracellular matrix composition[4]. Tissue stiffness, a measure of the resistance to deformation when force is applied, can vary by orders of magnitude from soft adipose tissue to stiff skeletal muscle[5]. However, while mechanical input during the formation of the immunological synapse is known to impact T cell receptor (TCR) signaling[6,7], it remains unclear whether activated T cells respond to

[1]Department of Physiology, McGill University, Montreal, Quebec, Canada. [2]McGill University Research Centre on Complex Traits, McGill University, Montreal, Quebec, Canada. [3]Department of Microbiology and Immunology, McGill University, Montreal, Quebec, Canada. [4]Department of Bioengineering, McGill University, Montreal, Quebec, Canada. [5]Department of Biochemistry, McGill University, Montreal, Quebec, Canada. [6]NYU Langone Transplant Institute, NYU Grossman School of Medicine, New York, NY, USA. [7]Division of Cardiology, McGill University Health Centre, Montreal, Quebec, Canada. [8]Courtois Cardiovascular Signature Program, McGill University Health Centre, Montreal, Quebec, Canada. [9]Center for Immunology, University of Minnesota, Minneapolis, MN, USA. [10]Data Science group, Institute for Computing and Information Sciences, Radboud University, Nijmegen, The Netherlands. [11]Alan Edwards Center for Research on Pain, McGill University, Montreal, Quebec, Canada. [12]DREAM-LAB, Research Institute of the McGill University Health Centre, Montreal, Quebec, Canada. [13]These authors contributed equally: Jérémy Postat, Mauricio Merino, Angela R. Mingarelli. e-mail: judith.mandl@mcgill.ca

differences in stiffness of the tissues through which they navigate, and thus whether physical changes in the microenvironment impact adaptive immunity.

Adherent cells respond to mechanical forces as they interact with surrounding substrates. External forces propagate through the cytoskeleton to the nucleus and lead to changes in the composition of the nuclear lamina, including the upregulation of lamin A/C, which increases the rigidity of the nucleus to protect the genomic material of the cell from force-mediated DNA damage[8,9]. Unlike tissue cells, T cells have to remain highly motile to exert their protective functions and thus presumably face an important trade-off: to survive long term they have to withstand tissue-imposed mechanical forces, yet need to remain able to undergo extreme shape deformations to squeeze around obstacles—a process in which nuclear rigidity is a rate-limiting step[10–12]. How activated T cells balance the need to remain motile while protecting their DNA and whether this impacts T cell fate in tissues remains unknown.

Mechanosensing in adherent tissue cells can result in cytoskeletal responses[13,14] and lead to gene expression changes, such as those mediated by YAP and TAZ—two transcriptional regulators implicated in translating mechanical cues into gene expression changes in many cell types[15,16]. Studies showing that mesenchymal stem cells become adipocytes on soft substrates versus osteocytes on stiff substrates indicate that mechanosensing can alter cell differentiation and therefore cell fate[15]. Here, we examined whether CD8$^+$ T cells integrated mechanical cues following activation and asked if this impacted their transcriptional state and thus ultimately their differentiation trajectory. By titrating mechanical input, we showed that mechanosensing in T cells in response to external force leads to cell cycle arrest for DNA repair, changes in nuclear envelope composition, altered cell morphology and modulated key transcription factors that mediate a T_{RM} cell-like transcriptional state.

Results

CD8$^+$ T cell morphology is altered in response to mechanical input

To investigate whether T cells responded to mechanical cues as they traversed complex three-dimensional (3D) microenvironments, we isolated CD8$^+$ T cells from spleen and lymph nodes (LN) (both soft tissues) of C57Bl/6 mice, activated them in media with CD3 + CD28 antibodies (Ab) for 2 days, expanded for an additional day with IL-2 (protocol used hereafter unless otherwise stated) and then embedded the cells in collagen matrices polymerized from bovine (soft) or rat tail (stiff) type I collagen for up to 24 h (Fig. 1a). Activated T cells spontaneously migrate within collagen gels without requiring integrin binding or the addition of chemokine[17]. As the most abundant extracellular matrix component, collagen crosslinking is key to modulating tissue stiffness. At equal concentrations, polymerized rat tail versus bovine collagen has distinct mechanical properties[18]. The stiff telo-rat tail collagen retains the telopeptide region that enables greater collagen fiber crosslinking and generates a less deformable matrix than the atelo-bovine collagen[19]. Nanoindentation showed that the telo-rat tail collagen was ~3-fold stiffer than the atelo-bovine collagen (Fig. 1b). A similar (~2-fold) difference was obtained when measuring the storage modulus by shear rheology (Extended Data Fig. 1a). A comparison of other mechanical properties[20] indicated that both types of collagen were predominantly elastic and fast relaxing, with no meaningful differences in viscoelastic properties (Extended Data Fig. 1a,b). Thus, assessment of T cell migration within bovine (soft) or rat tail (stiff) collagen could be used as a reductionist system to modulate mechanical input, while keeping other parameters constant.

In general, T cell motility in nonlymphoid tissues is slower than within lymphoid organs, a presumed function of tissue microarchitecture[21,22]. CD8$^+$ T cells had reduced speeds in the stiff compared to soft collagen (Fig. 1c). Mean cell speed in the soft collagen was unchanged between 8 and 24 h of migration, whereas in stiff collagen it decreased further by 24 h (Fig. 1c). This decreased CD8$^+$ T cell motility in stiff collagen was not accompanied by a change in cell viability (membrane integrity dye), and we observed only a minor increase (0.8% to 1.1%) in ApoTracker+ apoptotic CD8$^+$ T cells (Extended Data Fig. 1c,d). To ask whether cell-intrinsic, rather than environmental, changes impacted cell speed over time, we compared cell and nuclear morphology between T cells moving in stiff versus soft collagen. CD8$^+$ T cells isolated from spleen and LN of mice expressing both a fluorescent reporter for F-actin in all cells (LifeAct-eGFP mice) and a nucleus-localization signal-tagged Tdtomato (nTnG mice) were activated with CD3 + CD28 Ab, embedded in collagen and visualized

Fig. 1 | CD8$^+$ T cell migration in stiffer environments leads to altered cell morphology, decreased motility and increased nuclear lamin A/C expression. **a**, Experimental scheme showing naive CD44^{lo}CD8$^+$ T cells (T_N) isolated from spleen activated in media for 3 days with CD3 + CD28 Ab and then embedded into 3D gels made from 2 mg ml^{-1} bovine type I collagen (soft gel) or rat tail type I collagen (stiff gel), followed by isolation 8 h or 24 h later for functional assays. **b**, Collagen gel stiffness (Young's elastic modulus) measured by nanoindentation of soft and stiff collagen gels as in **a** (n = 6–7 gels per group). Assay detection limit, 40 Pa. **c**, The mean migration speed of CD8$^+$ T cells in soft versus stiff gels at 8 h (n = 1,361 cells, soft gel; n = 528 cells, stiff gel) or 24 h (n = 2,350 cells, soft gel; n = 650 cells, stiff gel) post-seeding. Group means are shown. Cells analyzed were isolated from three mice. **d**, Representative confocal microscopy images of 4 examples of activated CD8$^+$ T cells (n = 3 mice), from migrating in soft versus stiff gels for 24 h. F-actin (Lifeact reporter), nucleus (nTnG reporter) and collagen fibers are shown. **e**, PCA of 20 shape descriptors extracted from microscopy images of CD3 + CD28 Ab-activated CD8$^+$ T cells migrating in soft (n = 204 cells) versus stiff (n = 122 cells) gels for which cellular and nuclear shapes were quantified at 24 h post-migration. The 95% confidence intervals (CIs) of s.e.m. are shown. Cells analyzed were from three independent CD8$^+$ T cell cultures. **f**, Cell and nuclear shape outlines of CD8$^+$ T cells used for PCA as in **e**, sampled at random from a subpopulation of PC1 >|3| (nucleus) or PC2 >|3| (cell) and colored by area. **g**, Representative histograms and quantification of relative fluorescence intensity (RFI) normalized to the soft collagen condition mean (n = 18 mice, pooled from 4 independent experiments) of lamin A/C expression assessed by flow cytometry in mouse activated CD8$^+$ T cells migrating for 24 h in soft versus stiff gels as in **a**. **h**, Representative histograms and summarized RFI normalized to the soft collagen condition mean (n = 6 mice, pooled from 2 independent experiments) of lamin A/C expression assessed by flow cytometry in P14 TCR transgenic CD8$^+$ T cells activated with GP33 peptide-pulsed splenocytes for 3 days and then placed into soft versus stiff gels for 24 h. **i**, Max projection and representative z slices from confocal images of CD3 + CD28 Ab-activated CD8$^+$ T cells (n = 2 mice, representative of 4 experiments) migrating in soft versus stiff gels for 24 h as in **a**. **j**, Collagen gel stiffness (Young's elastic modulus) measured by nanoindentation of 1 mg ml^{-1}, 2 mg ml^{-1} and 3 mg ml^{-1} atelo- and telo-bovine collagen and 0.5 mg ml^{-1}, 1 mg ml^{-1} and 2 mg ml^{-1} telo-rat tail collagen (n = 4–6 gels per group). Median stiffness of the soft (2 mg ml^{-1} atelo-bovine) and stiff (2 mg ml^{-1} telo-rat tail) collagens as in **b**. **k**, Lamin A/C expression as assessed by flow cytometry in mouse CD3 + CD28 Ab-activated CD8$^+$ T cells migrating in collagen gels as in **j** (n = 6–10 mice, pooled from 2 independent experiments) for 24 h. RFI normalized to 2 mg ml^{-1} atelo-bovine collagen. **l**, Lamin A/C expression in human CD3 + CD28 Ab-activated CD8$^+$ T cells isolated from PBMC (n = 11 donors, pooled from 4 independent experiments) migrating in soft or stiff collagen gels for 24 h as in **a**. RFI normalized to the soft collagen condition mean. **m**, Lamin A/C expression assessed by flow cytometry in human CD3 + CD28 Ab-activated CD8$^+$ T cells (n = 4 donors) migrating in 0.5 mg ml^{-1}, 1 mg ml^{-1} and 2 mg ml^{-1} telo-rat tail collagen for 24 h. RFI normalized to 0.5 mg ml^{-1} telo-rat tail collagen condition per individual. Medians shown in all quantification plots. Error bars are median ± min/max with box boundaries denoting 25th and 75th percentiles (**b**,**g**,**j**,**k**,**m**). Statistical tests: Mann–Whitney (**b**), ANOVA with Dunn's multiple comparisons test (**c**), Wilcoxon (**g**,**h**,**l**), ANOVA with Tukey's correction for multiple comparisons (**k**) and ANOVA with Friedman test (**m**); all statistical tests were two sided; *P < 0.05, **P < 0.01, ***P < 0.001. n.d., not detectable (below 40 Pa); n.s., not significant.

https://doi.org/10.1038/s41590-026-02581-9

by confocal microscopy. At 24 h, cell and nuclear shapes of CD8$^+$ T cells visibly differed between stiff and soft collagen gels (Fig. 1d). Principal component analysis (PCA) of extracted cell and nuclear shape parameters from microscopy data separated stiff-embedded CD8$^+$ T cells from soft-embedded CD8$^+$ T cells in the PCA space at 24 h, but not 8 h (Fig. 1e and Extended Data Fig. 1e). Example outlines of CD8$^+$ T cells showed the cells were rounder and bigger, with larger nuclei in the stiff matrix, while CD8$^+$ T cells in soft gels were elongated, with more circular nuclei (Fig. 1f). A significant increase in the perimeter and area of the cells and their nuclei was observed in stiff compared to soft collagen at 24 h (Extended Data Fig. 1f).

Increases in nucleus size can be indicative of cellular mechanosensing[11,23]. A key response circuit to mechanical stress in mesenchymal cells leads to a more rigid nuclear envelope through changes to the nuclear lamina, primarily by increasing lamin A/C expression[11]. Leukocytes are thought to have low lamin A/C expression to enable

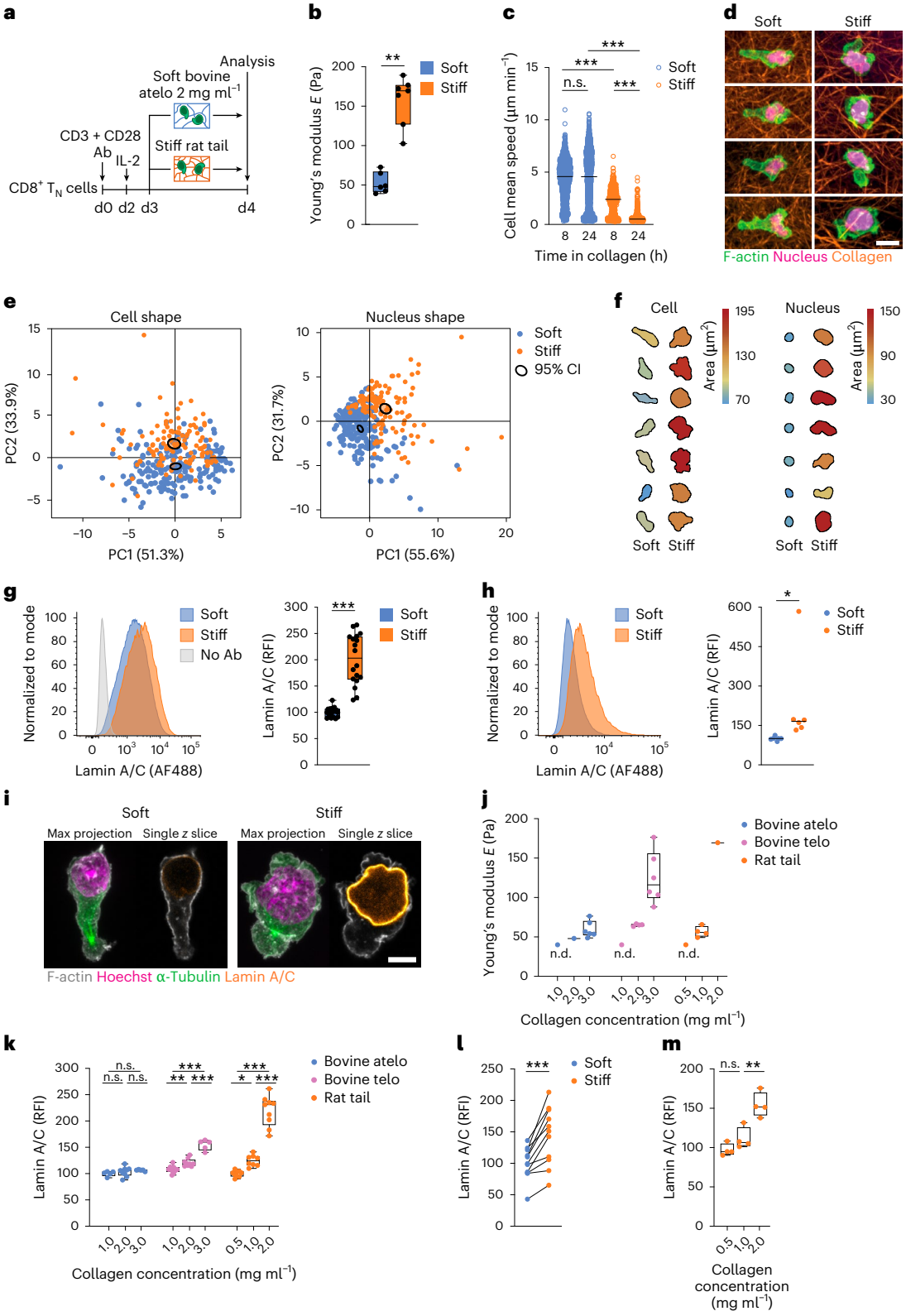

https://doi.org/10.1038/s41590-026-02581-9

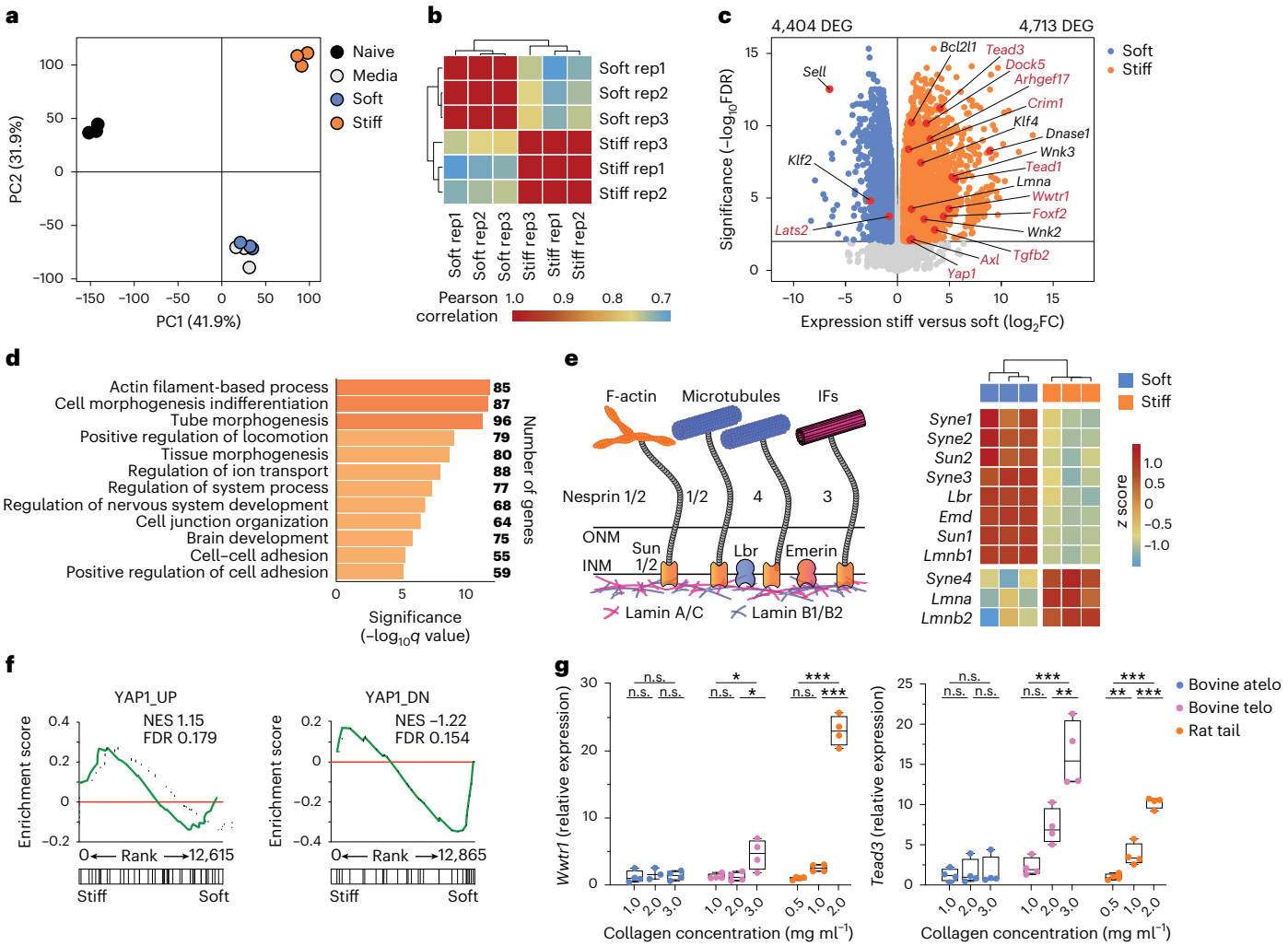

Fig. 2 | The CD8⁺ T cell transcriptome is altered in stiff collagen gels. a, PCA of RNA-seq from murine CD8⁺ T cell populations freshly isolated from spleen of WT mice or activated with CD3 + CD28 Ab in media for 3 days ($n = 3$ mice) and cultured in either media, soft (2 mg ml^{-1} atelo-bovine) or stiff (2 mg ml^{-1} telo-rat tail) collagen for 24 h. **b**,**c**, A CPM correlation matrix (**b**) and volcano plot (**c**) of significant DEGs (FDR <0.01) as in **a**. Positive FC values in the volcano plot indicate increased expression in CD8⁺ T cells isolated from the stiff gels. The number of DEGs and specific genes of interest (red data points) are indicated. Genes in the YAP/TAZ pathway are labeled in red. **d**, GO analysis of significant DEGs as in **c** at FC >2. A bar graph with gene numbers per category of the top nonredundant enrichment clusters identified with at least 50 genes is shown. **e**, A schematic of the proteins in the LINC complex and heat map of LINC gene expression identified among DEGs as in **c**. **f**, GSEA of upregulated (YAP1_UP MSigDB #M2845) and downregulated (YAP1_DOWN MSigDB #M2841) genes enriched in RNA-seq as in **a**. **g**, Expression of *Wwtr1* and *Tead3* determined by RT–qPCR in mouse CD8⁺ T cells activated in media with CD3 + CD28 Ab and embedded in 1 mg ml^{-1}, 2 mg ml^{-1} and 3 mg ml^{-1} atelo- and telo-bovine collagen or 0.5 mg ml^{-1}, 1 mg ml^{-1} and 2 mg ml^{-1} telo-rat tail collagen ($n = 4$ mice, pooled from 2 independent experiments) for 24 h. Relative expression is normalized to 1 mg ml^{-1} atelo-bovine collagen group. Error bars are median ± min/max with box boundaries denoting 25th and 75th percentiles; each data point is from an individual mouse (**a**,**g**). Statistical tests: ANOVA with Tukey's correction for multiple comparisons (**g**); all statistical tests were two sided; $^{*}P < 0.05$, $^{**}P < 0.01$, $^{***}P < 0.001$. IFs, intermediate filaments; INM, inner nucleus membrane; ONM, outer nucleus membrane; NES, normalized enrichment score.

better squeezing through physical obstacles in tissues[24]. However, T cells alter their nuclear rigidity and modulate lamin A/C expression[12]. CD8⁺ T cells migrating in stiff collagen had increased expression of lamin A/C protein compared to CD8⁺ T cells in soft collagen at 24 h (Fig. 1g). Lamin A/C upregulation in the stiff collagen was also observed in P14 TCR transgenic (lymphocytic choriomeningitis virus (LCMV)-specific) CD8⁺ T cells activated in vitro with GP33 peptide-pulsed splenocytes (Fig. 1h), suggesting this mechano-response was independent of activation mode. High-resolution microscopy indicated that the increase in nuclear lamin A/C expression in stiff-collagen-embedded CD8⁺ T cells was primarily in a thin layer around the nucleus (Fig. 1i), as described in adherent cells[9]. To rule out bovine versus rat collagen differences, we embedded activated CD8⁺ T cells in three collagens: atelo-bovine, telo-bovine and telo-rat tail collagen, each at three concentrations to further titrate gel stiffness (Fig. 1b,j). Lamin A/C expression was increased in the telo-bovine collagen of similar stiffness as the telo-rat tail collagen, as well as with increasing telo-bovine and rat tail collagen concentrations (Fig. 1j,k), indicating lamin A/C expression was mechanically regulated. Expression of lamin A/C also increased in CD3 + CD28 Ab-activated human CD8⁺ T cells isolated from peripheral blood mononuclear cells (PBMC) embedded in stiff compared to soft collagen (Fig. 1l), and scaled with the rat tail telo-collagen concentration used (Fig. 1m). Thus, CD8⁺ T cells responded to mechanical input from their microenvironment through changes in cell shape and nuclear lamina composition.

The CD8⁺ T cell transcriptome is altered in stiff microenvironments

To assess gene expression changes in response to environments of variable stiffness, we next performed RNA-sequencing (RNA-seq) on

mouse CD8$^+$ T cells activated in media with CD3 + CD28 Ab and transferred to stiff or soft collagen matrices or suspended in media for 24 h on day 3 after priming, making it unlikely that gene expression was modulated by mechanical input during activation. PCA and Pearson correlation revealed that CD8$^+$ T cells migrating in stiff gels had a distinct transcriptomic profile compared to CD8$^+$ T cells migrating in soft collagen or kept in media (Fig. 2a,b). We identified 9,117 differentially expressed genes (DEGs) comparing soft- versus stiff-embedded CD8$^+$ T cells (Fig. 2c and Supplementary Table 1), while CD8$^+$ T cells migrating in soft gels differed from cells in media by only 3 DEGs, *Fos*, *Fosb* and *Klf4* (Extended Data Fig. 2a,b), of which only the expression of *Klf4* increased further in stiff collagen (Extended Data Fig. 2c). *Lmna* (encodes lamin A/C) mRNA and protein expression were similar in media and soft gels (Extended Data Fig. 2d,e), suggesting CD8$^+$ T cells were subject to minimal mechanical input in soft gels despite active migration. Gene Ontology (GO) analysis of the 3,589 DEGs upregulated more than twofold in stiff versus soft gels identified an enrichment of genes related to 'actin filament-based process', 'positive regulation of locomotion' and 'cell–cell adhesion' (Fig. 2d). GO analysis also identified genes relating to 'tube morphogenesis', 'tissue morphogenesis' and 'ion transport', all of which were enriched for genes involved in mechanosensing by cells for their correct positioning and differentiation during development, including *Wnk2* and *Wnk3*, which regulate cell size (Fig. 2c,d). Conversely, many genes encoding members of the LINC complex, which mediates force transmission from the cell microenvironment to the nuclear envelope via the cytoskeleton[25,26], and nuclear lamina (*Syne1-4*, *Sun1-2*, *Lbr*, *Emd*, *Lmnb1* and *Lmnb2*) were downregulated in the stiff gels (Fig. 2e). In mesenchymal cells, downregulation of LINC proteins occurs in response to intense mechanical strain[27], suggesting downregulation of LINC complex genes in CD8$^+$ T cells in the stiff matrix was uncoupling the nucleus from the cytoskeleton to protect their DNA from mechanical damage.

Yap1 and *Wwtr1* (that encode YAP and TAZ) were among the DEGs upregulated in CD8$^+$ T cells in stiff compared to soft collagen (Fig. 2c). YAP and TAZ can bind to DNA only through interaction with TEAD coactivators[28], and *Tead1* and *Tead3*, as well as a number of YAP and/or TAZ target genes, including *Axl*, *Dock5*, *Arhgef17* and *Foxf2*[29], were significantly upregulated in CD8$^+$ T cells in stiff compared to soft gels (Fig. 2c). Gene set enrichment analysis (GSEA) indicated that genes upregulated by YAP were overrepresented in stiff gel-embedded CD8$^+$ T cells, while those downregulated were overrepresented in CD8$^+$ T cells migrating in soft gels (Fig. 2f). RT–qPCR indicated upregulation of *Wwtr1* and *Tead3* (Fig. 2g) and *Yap1* and *Tead1* (Extended Data Fig. 2f) in CD8$^+$ T cells with increasing bovine and rat tail telo-collagen concentrations, but not in atelo-bovine collagen, consistent with mechanical input being a key driver in changes in YAP/TAZ pathway genes. Overall, the CD8$^+$ T cell transcriptional response to increased mechanical input included changes in the expression of gene modules involved in mechanotransduction and response in other cells.

Mechanical input leads to cell cycle arrest and DNA repair

Mechanical stress applied to cardiomyocytes when lamin A/C upregulation is prevented leads to DNA damage and cell cycle arrest[8], while migration of dendritic cells or cancer cells through constrictions causes nuclear envelope ruptures, DNA leakage into the cytoplasm and subsequent DNA repair[30,31]. GSEA revealed that CD8$^+$ T cells migrating in stiff versus soft gels were enriched for genes in DNA repair-related p53 signaling, such as *Mdm2*, *Bax*, *Ccnd1*, *Rb1* and *Timp3* (Fig. 3a). To assess whether migration in stiff collagen led to DNA damage in CD8$^+$ T cells and whether this was actively being repaired to prevent cell death, we stained for γ-H2AX, a marker of double-stranded DNA breaks, as well as for phosphorylated checkpoint kinase 1 (Chk1), a key coordinator of the DNA damage response. We observed an increased frequency (3.1-fold) of γ-H2AX^{hi}CD8$^+$ T cells, as well as greater expression (1.6-fold) of pChk1 in stiff- compared to soft gel-embedded cells (Fig. 3b,c). Given that DNA lesions are rapidly repaired and γ-H2AX might therefore underestimate the extent of stiffness-induced DNA damage, we blocked DNA repair by the addition of NU7441, a selective DNA-PK inhibitor. While the frequency of γ-H2AX^{hi}CD8$^+$ T cells was unaffected and pChk1 expression increased slightly (1.2-fold) in the soft gel by NU7441 addition, both the frequency of γ-H2AX^{hi} cells and the expression of pChk1 in CD8$^+$ T cells further increased in stiff gels when DNA damage repair was inhibited, without greatly impacting cell numbers (Fig. 3b,c). pChk1 was highest in the γ-H2AX^{hi} population (Fig. 3b), suggesting γ-H2AX^{hi} cells marked cells with DNA damage accrued in response to stiffness, rather than cell division.

DNA repair is often accompanied by p53-mediated cell cycle pausing[32]. As we found a ~2-fold reduction in CD8$^+$ T cell numbers in stiff compared to soft gels without a large change in cell viability (Fig. 3c), we assessed DNA content with CytoPhase violet. A greater fraction of CD8$^+$ T cells in the stiff gels (53%) were in the G1 phase of the cell cycle compared to soft gels (27%) (Fig. 3d), suggesting reduced cell cycle progression with increased mechanical load. In addition, the p53 target *Cdkn1a* (encodes p21) and cell cycle inhibitor *Cdkn2a* (p16) were among the DEGs upregulated in CD8$^+$ T cells in stiff compared to soft gels (Fig. 3e), with the latter only expressed at very low counts per million (CPM) (Extended Data Fig. 3a). Expression of the anti-apoptotic factor Bcl-XL was increased in the stiff versus soft gels (Fig. 3f) and the frequency of cells with a high number of DNA breaks (score 3), measured with a comet assay, was twofold greater in stiff- compared to soft gel-embedded CD8$^+$ T cells, although at low frequencies (Fig. 3g), both suggestive of active DNA repair. To establish whether lamin A/C upregulation directly contributed to nuclear protection in CD8$^+$ T cells during migration, we generated hematopoietic cell-conditional *Lmna*-deficient (*lmna* cKO) mice by crossing *Lmna*$^{fl/fl}$ with Vav-Cre mice, and confirmed by flow cytometry that their T cells did not upregulate lamin A/C in stiff collagen (Extended Data Fig. 3b). We saw a similar upregulation in γH2AX and pChk1 (Fig. 3h), Bcl-XL and *Cdkn2a* (Extended Data Fig. 3c,d) between Vav-Cre$^-$*Lmna*$^{fl/fl}$ (wild type (WT))

Fig. 3 | Mechanosensing induces DNA damage and reduced cell cycle progression in CD8$^+$ T cells. a, GSEA of p53 signature (MSigDB #MM3896) performed on RNA-seq from CD3 + CD28 Ab-activated CD8$^+$ T cells ($n = 3$ mice) migrating in soft (2 mg ml^{-1} atelo-bovine) or stiff (2 mg ml^{-1} telo-rat tail) collagen for 24 h. **b**, Representative contour plot of γH2AX (DNA damage marker) and pChk1 (DNA lesion repair) expression measured by flow cytometry in mouse CD3 + CD28 Ab-activated CD8$^+$ T cells migrating in soft (2 mg ml^{-1} atelo-bovine) or stiff (2 mg ml^{-1} telo-rat tail) collagen in the presence of 2 μM NU7441 for 24 h. **c**, Quantification of γH2AX and pChk1 (left) and number of live CD8$^+$ T cells (right) in CD8$^+$ T cell migrating in soft and stiff gels with or without NU7441 as in **b** ($n = 8$ mice, pooled from 2 independent experiments). **d**, Representative histograms and quantification of DNA content measured by flow cytometry with CytoPhase violet in CD3 + CD28 Ab-activated CD8$^+$ T cells ($n = 8$ mice, pooled from 2 independent experiments) migrating in soft versus stiff gels as in **a**. **e**, Expression of *Cdkn1a* in RNA-seq of activated CD8$^+$ T cells ($n = 3$ mice) from soft versus stiff collagen gels as in **a**. The lines denote means per group. **f**, Representative histogram and quantification of Bcl-XL expression measured by flow cytometry in CD3 + CD28-activated CD8$^+$ T cells ($n = 8$ mice, pooled from 2 independent experiments) migrating in soft versus stiff gels as in **a**. **g**, Representative images of visual scoring (left) and distribution (right) of alkaline comet assay of CD8$^+$ T cells migrating in soft ($n = 865$ cells) and stiff ($n = 626$ cells) gels for 24 h as in **a**. **h**, Expression of γH2AX and pChk1 measured by flow cytometry in WT or *Lmna* cKO CD8$^+$ T cells activated with CD3 + CD28 Abs in media for 3 days and embedded in soft or stiff collagen as in **a** for 24 h ($n = 7$ mice, pooled from 2 independent experiments). Medians are shown in all quantification plots (**c**–**f**,**h**); each data point is from an individual mouse. Statistical tests: ANOVA with Holm–Šídák's correction for multiple comparisons (**c**,**d**), Wilcoxon (**g**), ANOVA with Dunn's multiple comparisons test (**h**); all statistical tests were two sided; $^{**}P < 0.01$, $^{***}P < 0.001$. PE, phycoerythrin.

https://doi.org/10.1038/s41590-026-02581-9

littermates and *Lmna* cKO CD8$^+$ T cells in stiff gels. Thus, migration in stiff environments led to DNA damage, reduced cell cycle progression and elicited a DNA repair response in CD8$^+$ T cells, independent of lamin A/C expression, at least in the short term.

Responses to mechanical cues drive a CD8$^+$ T_{RM} cell-like state

To better understand the range of tissue stiffness experienced by CD8$^+$ T cells in vivo, we compared the Young's elastic modulus of secondary lymphoid organs to other tissues in C57Bl/6 mice. Liver, lung, kidney and salivary gland were ~10-fold stiffer (2.2 kPa) than LN and spleen (0.2 and 0.4 kPa, respectively) (Fig. 4a). In addition, at the peak of the effector T cell response (day 7) following LCMV infection, spleen stiffness was increased ~6-fold compared to uninfected controls (Fig. 4b), as also seen in LN[33], indicating that upon infection, effector T cells experience greater mechanical input both within secondary lymphoid organs and in transit to other tissues. To assess whether stiffness sensing contributed to T_{RM} cell differentiation, we compared gene expression differences in the soft- versus stiff-embedded CD8$^+$ T cells RNA-seq (mechanosensitive transcriptome) to a 'core CD8$^+$ T_{RM} cell-associated' gene list of 57 genes previously defined in CD8$^+$ T_{RM} cells in lung, gut,

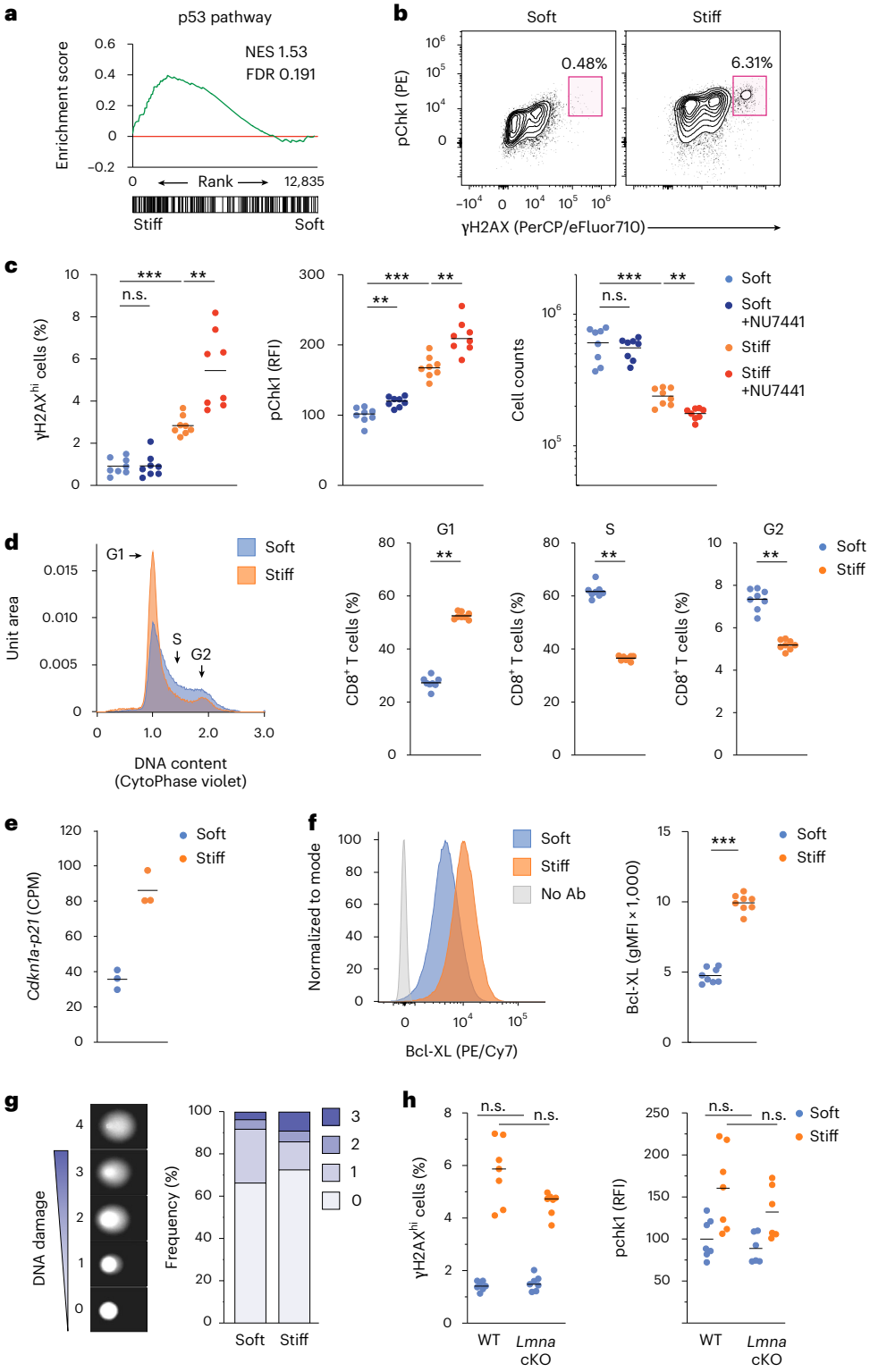

liver and skin of mice relative to circulating CD8$^+$ T_{CM} and effector CD8$^+$ T cells[34–36] (Supplementary Table 2). This core CD8$^+$ T_{RM} cell program includes the downregulation of genes involved in recirculation and lymphoid organ entry, such as *Sell* (encoding CD62L), *Ccr7* and receptors for S1P (*S1pr1* and *S1pr5*), and the increased expression of adhesion molecules, including *Cd69*, *Itgae* (encoding CD103) and *Itga1* (encoding CD49a). GSEA of the mechanosensitive transcriptome showed that core upregulated T_{RM} cell genes were significantly enriched in CD8$^+$ T cells migrating in stiff gels, while core downregulated T_{RM} cell genes were significantly enriched in cells migrating in soft gels (Fig. 4c). Of the 57 genes in the core CD8$^+$ T_{RM} cell list, 55 were detected and 42 were among the DEGs in the mechanosensitive transcriptome (Fig. 4d). Of the 21 genes upregulated in the core T_{RM} cell program, 14 were significantly up in CD8$^+$ T cells in the stiff compared to soft matrix, including adhesion molecules *Cdh1* and *Itga1*, chemokine *Xcl1* and costimulatory molecule *Icos* (Fig. 4d). Of the 21 genes downregulated in the core T_{RM} cell program, 19 were significantly down in stiff matrix-embedded CD8$^+$ T cells (Fig. 4d). We also examined 21 additional genes upregulated in CD8$^+$ T_{RM} cells manually curated from published studies[37–39] (Supplementary Table 2). This included *Lmna*, which has been reported to be upregulated in lung CD8$^+$ T_{RM} cells[40], but also *Ahr*, *Bach2*, *Fosl2*, *Pdcd1* and others, all of which were upregulated in stiff-embedded CD8$^+$ T cells (Fig. 4d).

To assess whether mechanical input altered the generation of effector CD8$^+$ T cells as well as driving a T_{RM} cell-like transcriptional state, we performed additional GSEA of the RNA-seq data. In contrast to T_{RM}-associated genes, soft gel CD8$^+$ T cells were significantly enriched for T cell activation- and effector cell-associated genes such as *Gzma*, *Irf4*, *Egr1*, *Ccr2* and *Il6ra* compared to stiff gel cells (Fig. 4e,f and Extended Data Fig. 4a). No significant differences were detected in the expression of granzyme B or perforin mRNA or protein between soft and stiff gel CD8$^+$ T cells, irrespective of whether T cells were activated with CD3 + CD28 Ab or with peptide-pulsed splenocytes (Fig. 4g and Extended Data Fig. 4b–d). Moreover, the effector cytokine genes *Tnf* and *Ifng* were expressed at similar levels in soft and stiff gel CD8$^+$ T cells (Extended Data Fig. 4e) and restimulation of soft or stiff gel-embedded CD8$^+$ T cells induced similar production of IFNγ or TNF (Fig. 4h and Extended Data Fig. 4f).

To investigate whether differences in the genes associated with a CD8$^+$ T_{RM} cell-like program translated to protein expression changes, and to test our findings in atelo-bovine, telo-bovine and telo-rat tail collagens across titrated concentrations as before, we used flow cytometry to measure expression of CD62L, which plays a role in recirculating between blood and lymphoid organs and is downregulated in CD8$^+$ T_{RM} cells and ICOS, which promotes CD8$^+$ T_{RM} cell generation[41], in CD3 + CD28 Ab-activated CD8$^+$ T cells embedded in collagen for 24 h. The percent of CD62L$^+$CD8$^+$ T cells decreased significantly with increased stiffness (from 95% in soft to 60% in stiff collagen), as did the fluorescence intensity of CD62L expression (Fig. 4i,j). Downregulation of CD62L was also observed in P14 CD8$^+$ T cells activated with GP33-pulsed splenocytes and embedded in stiff compared to soft collagen for 24 h (Fig. 4k). Conversely, ICOS expression increased by ~3-fold in CD8$^+$ T cells exposed to the stiffest collagen (3 mg ml^{-1} telo-bovine and 2 mg ml^{-1} telo-rat tail) gels compared to the soft atelo-bovine collagen (1, 2 or 3 mg ml^{-1}) (Fig. 4l). ICOS upregulation in stiff compared to soft-embedded cells was also observed in GP33 peptide-activated P14 CD8$^+$ T cells (Fig. 4m), suggesting that expression of ICOS and CD62L was modulated by the mechanical forces, regardless of whether T cells were activated by CD3 crosslinking or peptide stimulation. RT–qPCR of human CD8$^+$ T cells isolated from PBMC, activated with CD3 + CD28 Ab and embedded in soft versus stiff collagen for 24 h showed the core T_{RM}-associated genes *XCL1* and *ITGA1* were significantly upregulated in stiff versus soft gels (Fig. 4n). Thus, activated mouse and human CD8$^+$ T cells exposed to stiff environments acquired a T_{RM} cell-like state.

TGFβ does not drive the mechano-induced T_{RM}-like phenotype

TGFβ is implicated in CD8$^+$ T_{RM} cell differentiation in epithelial tissues (for example, skin), but dispensable for CD8$^+$ T_{RM} cell development in other organs (for example, liver)[42]. On the basis of the existence of a core transcriptional program in all CD8$^+$ T_{RM} cells regardless of tissue location[34–39], we tested whether there was overlap between mechano-induced and TGFβ-induced transcripts, including some of the 'core CD8$^+$ T_{RM} cell' genes. GSEA for Smad3 and Smad4, two transcriptional regulators downstream of TGFβ receptor binding[43], showed an enrichment of Smad3/4-regulated genes in stiff gel-embedded CD8$^+$ T cells (Extended Data Fig. 5a,b). TGFβ was undetectable in both soft and stiff collagen by ELISA (Extended Data Fig. 5c). Genes such as *Itgae*, *Tcf7* and *Hpgds*, described to be tissue dependent in CD8$^+$ T_{RM} cells due to differences in TGFβ availability[44], were not significantly different in the soft versus stiff collagen-embedded CD8$^+$ T cell RNA-seq (referred to as the 'mechanosensitive transcriptome'). Comparison of the DEGs from the mechanosensitive transcriptome to genes induced in peptide-activated

Fig. 4 | Responses to mechanical cues drive a CD8$^+$ T_{RM} cell-like state. **a**, Stiffness (Young's elastic modulus) of lymphoid (inguinal LN and spleen) and nonlymphoid (liver, lung, kidney and salivary gland (SG)) tissues from WT mice measured by nanoindentation (n = 5 or 6 mice for each tissue). **b**, Stiffness (Young's elastic modulus) of spleen tissue from uninfected or LCMV-Armstrong infected mice on day 7 post infection measured by nanoindentation (n = 5 mice per group). **c**, GSEA of genes upregulated (T_{RM} core UP) or downregulated (T_{RM} core DN) in the T_{RM} cell core gene signature (Supplementary Table 2) enriched in RNA-seq from CD3 + CD28 Ab-activated CD8$^+$ T cells (n = 3 mice) migrating in soft (2 mg ml^{-1} atelo-bovine) or stiff (2 mg ml^{-1} telo-rat tail) collagen. **d**, Heat map of T_{RM} cell core (T_{RM} core UP and T_{RM} core DN) signature genes as in **c**, and manually curated upregulated genes in CD8$^+$ T_{RM} cells (other T_{RM} genes UP) from the DEGs identified by RNA-seq in CD3 + CD28 Ab-activated CD8$^+$ T cells (n = 3 mice) migrating in soft versus stiff collagen as in **c**. **e**, GSEA of T cell activation genes (GO:0042110) enriched in DEGs in RNA-seq from CD8$^+$ T cells (n = 3 mice) migrating in soft versus stiff collagen for 24 h. **f**, GSEA of T effector genes[56] (GSE9650) enriched in DEGs from soft versus stiff RNA-seq as in **e**. **g**, Representative histogram and quantification of granzyme B expression in mouse naive CD8$^+$ T cells and CD3 + CD28 Ab-activated CD8$^+$ T cells migrating in soft and stiff collagen measured by flow cytometry (n = 7 mice, pooled from 2 independent experiments). **h**, Intracellular cytokine staining for IFNγ and TNF following PMA + ionomycin stimulation of CD3 + CD28 Ab-activated CD8$^+$ T cells (n = 9 mice, pooled from 2 independent experiments) migrating in soft versus stiff collagen for 24 h. **i**,**j**, Representative flow plot (**i**) and quantification of the percent of CD62L$^+$ cells and CD62L RFI, normalized to the 1 mg ml^{-1} atelo-bovine collagen mean (**j**) in CD8$^+$ T cells activated with CD3 + CD28 Ab and embedded in 1 mg ml^{-1}, 2 mg ml^{-1} and 3 mg ml^{-1} atelo- and telo-bovine collagen, and 0.5 mg ml^{-1}, 1 mg ml^{-1} and 2 mg ml^{-1} telo-rat tail collagen (n = 5 mice from 1 representative experiment) for 24 h. **k**, Expression of CD62L measured by flow cytometry in P14 CD8$^+$ T cells activated with GP33-pulsed splenocytes (n = 6 mice, pooled from 2 independent experiments) following migration in soft versus stiff collagen for 24 h. RFI normalized to the mean of cells in 2 mg ml^{-1} atelo-bovine collagen. **l**, Representative histogram and quantification of ICOS expression measured by flow cytometry in activated CD8$^+$ T cells embedded in collagen (n = 5 or 9 mice, pooled from 2 independent experiments) as in **i**. RFI normalized to the mean of cells in 2 mg ml^{-1} atelo-bovine collagen. **m**, ICOS expression in P14 CD8$^+$ T cells (n = 6 mice, pooled from 2 independent experiments) following migration in soft versus stiff collagen for 24 h as in **k**. RFI normalized to the mean of cells in 2 mg ml^{-1} atelo-bovine collagen. **n**, Expression of *XCL1* and *ITGA1* in human CD3 + CD28 Ab-activated CD8$^+$ T cells (n = 9 donors, pooled from 2 independent experiments) migrating in soft versus stiff collagen for 24 h was assessed by RT–qPCR, normalized to a housekeeping gene and shown as FC relative to the mean of the soft collagen condition. Medians are shown in all quantification plots (**g**,**h**,**k**,**m**). Error bars are median ± min/max with box boundaries denoting 25th and 75th percentiles (**a**,**b**,**j**,**l**,**n**). Statistical tests: ANOVA with Dunnett's correction for multiple comparisons (**a**), Mann–Whitney (**b**), ANOVA with Tukey's correction for multiple comparisons (**k**,**m**), Wilcoxon (**h**,**i**,**l**,**n**); all statistical tests were two sided; $^*P < 0.05$, $^{**}P < 0.01$, $^{***}P < 0.001$.

https://doi.org/10.1038/s41590-026-02581-9

transgenic CD8$^+$ T cells from spleen treated with TGFβ for 40 h 5 days after activation[44] indicated that 627 of the 9,117 stiffness-induced DEGs in the mechanosensitive transcriptome overlapped with TGFβ-induced DEGs (Extended Data Fig. 5d and Supplementary Table 3). There was a high degree of concordance among genes regulated both by stiffness and TGFβ, with genes upregulated by stiffness also upregulated by TGFβ (including *Itga1* and *Icos*) and stiffness-downregulated genes also downregulated by TGFβ (including *Arhgef18* and *Cdc25b*) (Extended Data Fig. 5e). Gene set comparisons indicated that some 'core CD8$^+$ T_{RM} cell' genes were only modulated by mechanical input, including *Klf2*, *S1pr1* and *S1pr4*, which were downregulated by stiffness and not by TGFβ (Supplementary Table 3).

To test the contribution by TGFβ in regulating the gene expression differences observed in collagen-embedded CD8$^+$ T cells, we used RT–qPCR to measure the changes in gene expression of six selected genes (*Hpgds*, *Nr4a2*, *Osgin1*, *Cdh1*, *Arhgef18* and *Cdc25b*) in CD3 + CD28 Ab-activated CD8$^+$ T cells embedded in soft versus stiff gels as before for 24 h with the addition of either TGFβ neutralizing antibody or

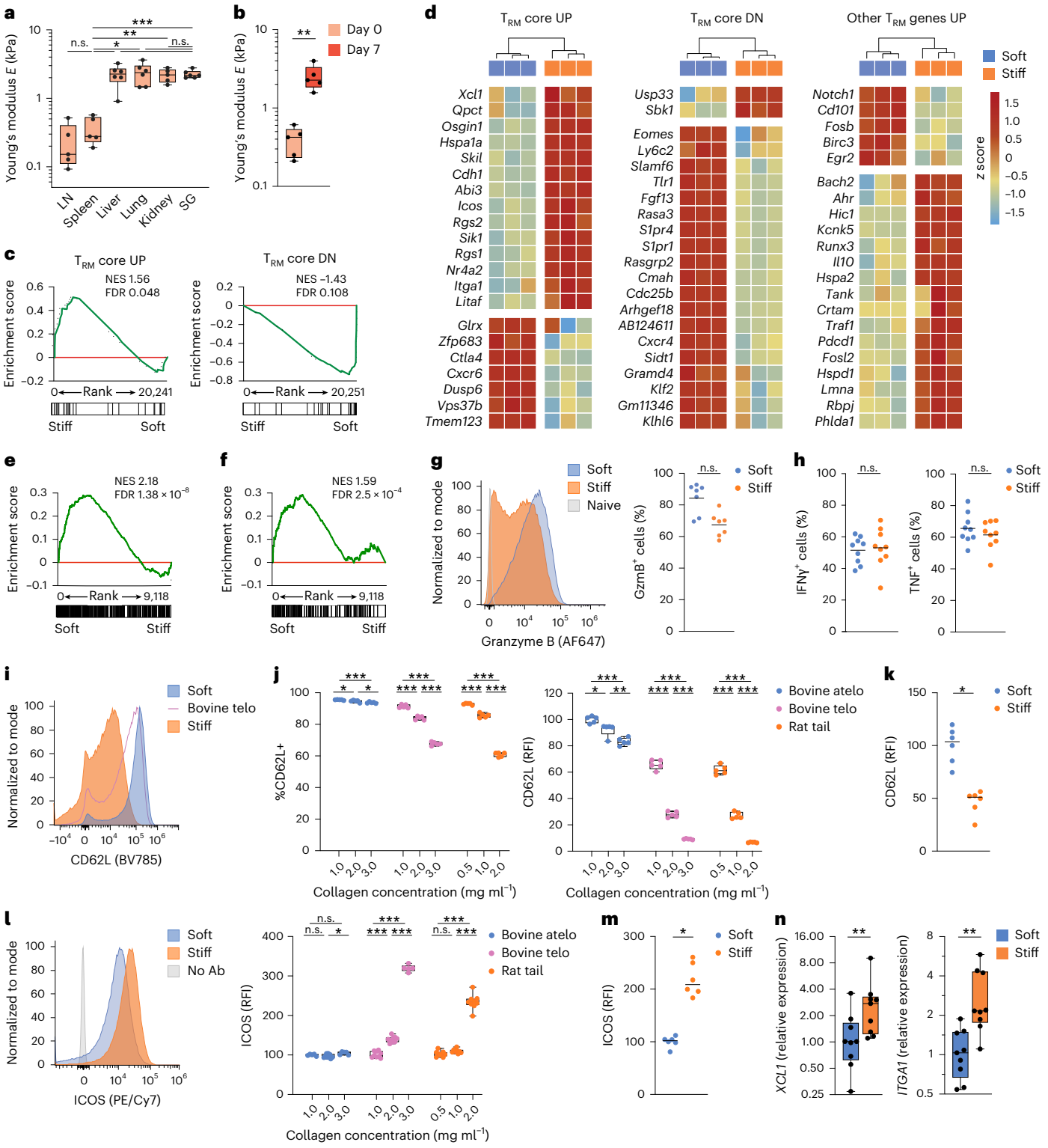

recombinant TGFβ during gel polymerization. Expression of *Hpgds* and *Nr4a2* were used as controls as the mechanosensitive transcriptome analysis indicated that *Hpgds* was only responsive to TGFβ, while *Nr4a2* was only responsive to stiffness (Supplementary Table 3). As expected, *Hpgds* was upregulated in soft or stiff gel-embedded CD8$^+$ T cells to which recombinant TGFβ was added, but not in CD8$^+$ T cells migrating in the absence of recombinant TGFβ (Extended Data Fig. 5f). By contrast, *Nr4a2* was significantly upregulated in stiff versus soft gel-embedded CD8$^+$ T cells, independent of addition of recombinant TGFβ or TGFβ antibody (Extended Data Fig. 5f). Based on comparisons of the TGFβ[44] and stiffness-induced genes in CD8$^+$ T cells, *Osgin1* and *Cdh1* were upregulated, while *Arhgef18* and *Cdc25b* were downregulated by both stiffness and TGFβ (Supplementary Table 3). RT–qPCR indicated that expression of *Osgin1* and *Cdh1* was higher in soft gel-embedded CD8$^+$ T cells only when recombinant TGFβ was added to the collagen, compared to soft gel-embedded CD8$^+$ T cells without TGFβ added, and was upregulated in stiff compared to soft collagen-embedded CD8$^+$ T cells even upon addition of TGFβ antibody (Extended Data Fig. 5g), indicating that both mechanical input and TGFβ signaling modulated *Osgin1* and *Cdh1* gene expression but that TGFβ was not responsible for the upregulation of these genes in stiff collagen. Similarly, RT–qPCR measured expression of *Arhgef18* and *Cdc25b* was lower in stiff compared to soft gel-embedded CD8$^+$ T cells, independent of the addition of TGFβ blocking antibody (Extended Data Fig. 5g), indicating that also for these downregulated genes, TGFβ was not mediating the stiffness-induced gene changes.

Last, because retinoic acid promotes CD8$^+$ T_{RM} cell formation in the liver and small intestine, but not the skin[45], we quantified the amount of retinoic acid in the atelo-bovine, telo-bovine and telo-rat tail collagen. Retinoic acid was detected at similar levels (~200 pg ml^{-1}) across all gels (Extended Data Fig. 5h). Thus, while genes impacted by gel stiffness in activated CD8$^+$ T cells overlapped with genes modulated by TGFβ, neither TGFβ nor retinoic acid was responsible for the stiffness-induced gene expression changes in activated CD8$^+$ T cells.

T_{RM}-like cells are generated in absence of defined mechanosensors

As YAP/TAZ function as transcriptional regulators during mechanotransduction[16], we examined whether the abrogation of YAP/TAZ signaling impacted the mechano-regulation of CD8$^+$ T_{RM} cell formation using two approaches. WT CD8$^+$ T cells isolated from spleen and LN and activated in media with CD3 + CD28 for 3 days were embedded in soft or stiff collagen polymerized with or without verteporfin, which blocks the interaction of YAP with Tead coactivators, and cells were left to migrate for 24 h. Expression of lamin A/C and ICOS was similarly upregulated, while CD62L downregulated in verteporfin-treated compared to untreated stiff-embedded CD8$^+$ T cells (Extended Data Fig. 6a–d). The stiffness-induced change in lamin A/C, CD62L and ICOS expression was similar in CD8$^+$ T cells from the spleen and LN of Tat-cre-treated *Yap1*$^{fl/fl}$*Wwtr1*$^{fl/fl}$ (YAP/TAZ dKO) or Tat-cre-treated *Yap1*$^{+/+}$*Wwtr1*$^{+/+}$ (WT) activated with CD3 + CD28 Abs in atelo-bovine, telo-bovine or telo-rat tail collagen (Extended Data Fig. 6e–h). To test whether the generation of T_{RM}-like cells was integrin dependent, given the role for integrins in mechanosensing across many cell types[23,46], spleen CD8$^+$ T cells from Tat-Cre-treated *Talin1*$^{fl/fl}$ mice (Talin cKO cells) were activated and embedded in atelo-bovine, telo-bovine or telo-rat tail collagen for 24 h. We found no differences in stiffness-induced lamin A/C, CD62L or ICOS expression (Extended Data Fig. 6i–k), indicating integrins were not required for the stiffness-induced upregulation of lamin A/C or the CD8$^+$ T_{RM} cell-like phenotype.

The Ca^{2+}-dependent phospholipase $cPLA_2$ can be triggered by mechanical forces[13,14] and enables sensing physical confinement by CD8$^+$ T_{RM} cells during tissue surveillance[21]. CD8$^+$ T cells treated with the $cPLA_2$ inhibitor AACOCF3 showed similar stiffness-induced changes in lamin A/C, CD62L and ICOS expression as in nontreated CD8$^+$ T cells embedded in stiff versus soft gels (Extended Data Fig. 6l–o). Physical confinement of cells triggers cytoskeleton contractility via myosin II downstream of $cPLA_2$ activation as a result nuclear envelope unfolding[13,14] and cytoskeletal processes can impact, and are themselves mediators of, cellular force sensing. For instance, in activated CD8$^+$ T cells, mechanical force leads to the redistribution of F-actin toward the cell center to protect the nucleus[12]. Inhibition of myosin II with blebbistatin in activated CD8$^+$ T cells embedded in stiff collagen led to an elongated cell morphology (Extended Data Fig. 7a), as described in dendritic cells[47], but did not impair the mechano-induced upregulation of lamin A/C and ICOS (Extended Data Fig. 7b,c), downregulation of CD62L (Extended Data Fig. 7d) or changes in expression of other CD8$^+$ T_{RM}-associated genes (Extended Data Fig. 7e) compared to DMSO-treated stiff collagen-embedded CD8$^+$ T cells. CD8$^+$ T cells treated with latrunculin B, which inhibits actin polymerization by sequestering G-actin monomers substantially impaired CD8$^+$ T cell motility in collagen, as expected (Extended Data Fig. 7f), but also greatly impacted CD8$^+$ T cell viability, with most CD8$^+$ T cells in stiff gels dead within 24 h post-treatment, precluding assessment of changes in protein or gene expression (Extended Data Fig. 7g). Lamin A/C expression has also been implicated in modulating gene expression changes during mechanotransduction[11,24]. However, *Lmna* cKO stiff collagen-embedded CD8$^+$ T cells differentiated into CD8$^+$ T_{RM}-like cells similarly to WT stiff collagen-embedded activated CD8$^+$ T cells (Extended Data Fig. 7h–k). Together, these data ruled out a role for previously identified mechanotransduction pathways in the generation of stiffness-induced T_{RM}-like cells.

Fig. 5 | The expression of transcription factors involved in T_{RM} differentiation is modulated by mechanical input. a, GSEA of Runx3-regulated genes (MSigDB #MM15520) performed on RNA-seq from CD3 + CD28 Ab-activated CD8$^+$ T cells ($n = 3$ mice) migrating in soft (2 mg ml^{-1} atelo-bovine) or stiff (2 mg ml^{-1} telo-rat tail) collagen for 24 h. **b**, Representative histogram and quantification of Runx3 expression measured by flow cytometry in CD3 + CD28 Ab-activated CD8$^+$ T cells embedded in 1 mg ml^{-1}, 2 mg ml^{-1} and 3 mg ml^{-1} atelo- and telo-bovine collagen, and 0.5 mg ml^{-1}, 1 mg ml^{-1} and 2 mg ml^{-1} telo-rat tail collagen ($n = 5$ or 9 mice, pooled from 2 independent experiments) for 24 h. RFI normalized to 2 mg ml^{-1} atelo-bovine collagen mean. **c**, Expression of Runx3 measured by flow cytometry in P14 CD8$^+$ T cells activated with GP33-pulsed splenocytes ($n = 6$ mice, pooled from 2 independent experiments) after migrating in soft versus stiff gels for 24 h. RFI normalized to soft collagen mean. **d**,**e**, Expression of *RUNX3* quantified by RT–qPCR (**d**) or flow cytometry (**e**) in human CD3 + CD28 Ab-activated CD8$^+$ T cells migrating in soft versus stiff gels for 24 h ($n = 5$ (**d**) or $n = 7$ (**e**) donors, pooled from 2 independent experiments). **f**,**g**, Expression of *Hic1* (**f**) and *Klf2* (**g**) quantified by RT–qPCR in CD3 + CD28 Ab-activated CD8$^+$ T cells ($n = 4$ mice) embedded in collagen as in **b** for 24 h. **h**,**i**, Representative histograms (**h**) and quantification (**i**) of KLF2–GFP reporter expression measured by flow cytometry in CD3 + CD28 Ab-activated CD8$^+$ and CD4$^+$ T cells ($n = 3$ mice, representative of 2 independent experiments) migrating in 2 mg ml^{-1} atelo-bovine, and 0.5 mg ml^{-1}, 1 mg ml^{-1} and 2 mg ml^{-1} telo-rat tail collagen for 24 h. **j**, Schematic showing the seeding of CD3 + CD28 Ab-activated KLF2–GFP$^+$ T cells onto fibronectin-coated glass slides with or without an agarose pad on top for 24 h followed by quantification of GFP in nucleus and cytoplasm. **k**, Representative microscopy image of KLF2–GFP$^+$ T cells placed under confinement under 0.5% agar pads as in **j**. Red outline, nuclear KLF2–GFP signal; white outline, cytoplasmic KLF2–GFP signal. Scale bar, 10 µm. **l**, Quantification of CD8$^+$ T cells with nuclear KLF2–GFP localization as in **k** that were unconfined ($n = 62$ cells), under 0.5% agar ($n = 105$ cells) or under 2% agar ($n = 103$ cells). **m**, Expression of T_{RM}-associated transcription factors (from ref. 52 in the DEGs assessed by RNA-seq in activated CD8$^+$ T cells migrating in soft versus stiff gels ($n = 3$ mice)). Medians shown in all quantification plots (**c**,**e**,**i**). Error bars are median ± min/max with box boundaries denoting 25th and 75th percentiles (**b**,**d**,**f**,**g**). Statistical tests: ANOVA with Tukey's correction for multiple comparisons (**b**,**f**,**g**), Wilcoxon (**c**–**e**), Benjamini–Hochberg method with FDR <0.01 (**m**). All statistical tests were two sided; $^*P < 0.05$, $^{**}P < 0.01$, $^{***}P < 0.001$.

https://doi.org/10.1038/s41590-026-02581-9

T_{RM}-associated transcription factors are mechanically modulated

We next investigated whether any of the transcriptional regulators shown to play a lineage-defining role in $CD8^+$ T_{RM} formation were among the DEGs in the mechanosensitive transcriptome. We focused on *Runx3* and *Hic1*, whose increased expression supports a T_{RM} program in $CD8^+$ T cells[37,38,48], and KLF2, whose downregulation contributes to T_{RM} cell tissue retention[3,49]. GSEA indicated that transcripts of Runx3-regulated genes, such as *Itga4*, *Tead1* and *Cdkn1a*, were enriched in stiff versus soft gel-embedded $CD8^+$ T cells (Fig. 5a). Expression of Runx3 protein in CD3 + CD28 Ab-activated collagen-embedded $CD8^+$ T cells increased with increasing collagen gel concentration in both telo-bovine and telo-rat tail collagen, and remained unchanged in atelo-bovine collagen, regardless of the collagen concentration (Fig. 5b). Expression of Runx3 protein was also upregulated in response to mechanical input in GP33-activated P14 T cells (Fig. 5c). We found a similar mechanical force-induced increase in RUNX3 expression at the gene and protein level in CD3 + CD28 Ab-activated human $CD8^+$ T cells isolated from PBMC and embedded in stiff rat tail versus soft bovine atelo-collagen (Fig. 5d,e). Using RT–qPCR, we found that *Hic1* gene expression

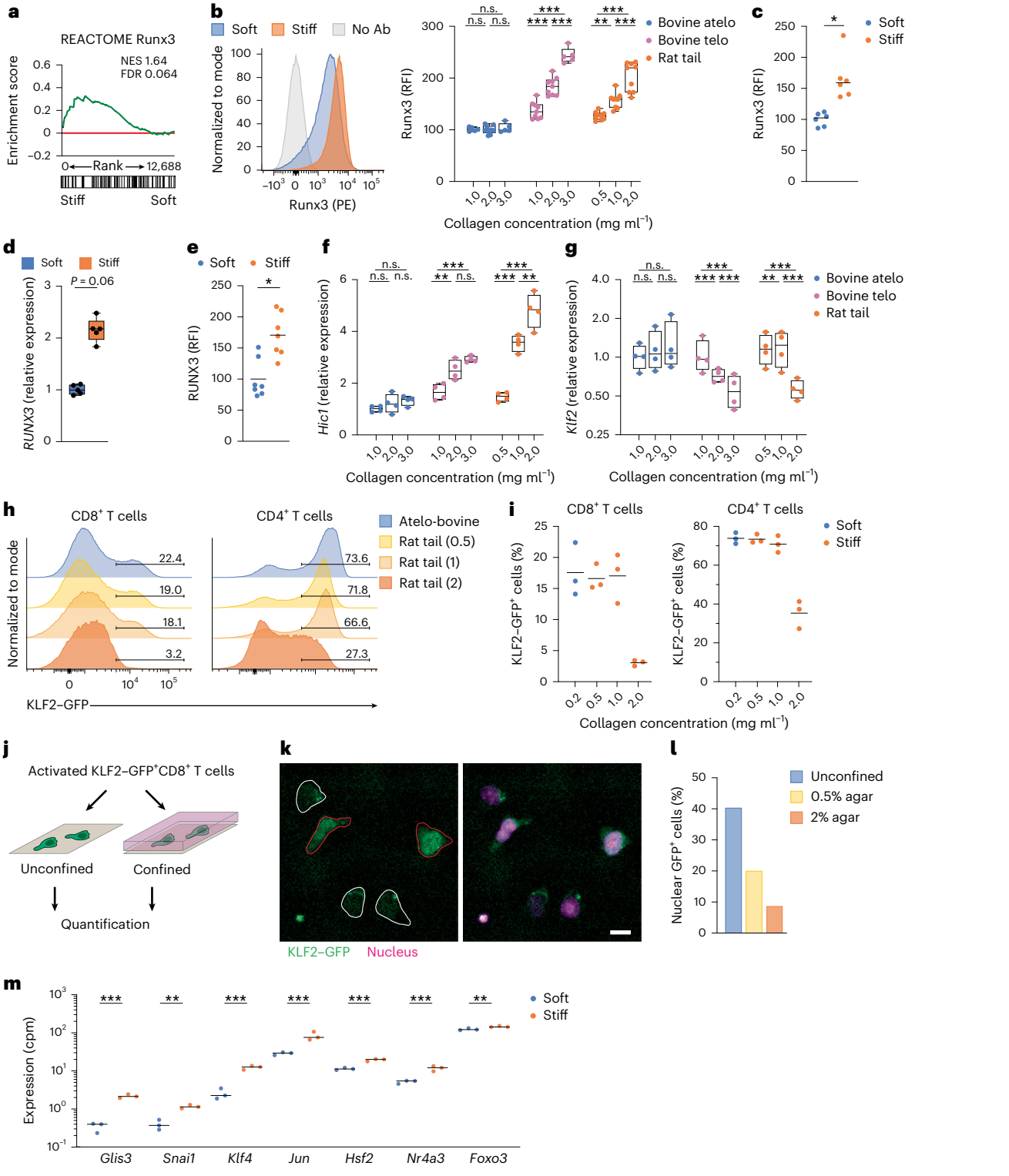

increased threefold in the stiffest telo-bovine collagen and fivefold in the stiffest telo-rat tail collagen compared to atelo-bovine (Fig. 5f).

KLF2 is mechanically regulated in vascular endothelial cells, mediating transcriptional responses to shear flow[50]. *Klf2* gene expression was downregulated in mouse CD3 + CD28 Ab-activated CD8$^+$ T cells in telo-bovine or rat tail stiff gels compared to atelo-bovine gels (Fig. 5g). CD8$^+$ and CD4$^+$ T cells isolated from spleens of KLF2–GFP reporter mice[51] and activated as before maintained expression of KLF2–GFP in low-stiffness gels, but downregulated expression in high-stiffness rat tail collagen (Fig. 5h,i). To assess KLF2 protein expression in T cells exposed to a different type of mechanical input, we also performed under-agarose migration assays, in which the mechanical load can be titrated by increasing the percent agarose used[12] (Fig. 5j). In the absence of agarose (unconfined migration) KLF2–GFP was primarily nucleus located, while in T cells loaded with 0.5% or 2% agarose, expression of KLF2–GFP decreased and the KLF2–GFP signal shifted from nuclear to cytoplasmic (Fig. 5k,l). In addition, among DEGs in the mechanosensitive transcriptome, we detected significant increases in other transcription factors associated with CD8$^+$ T_{RM} cell programming[52], including *Glis3*, *Snai1*, *Klf4*, *Jun*, *Hsf2*, *Nr4a3* and *Foxo3* (Fig. 5m). These findings established that the T_{RM} cell-like transcriptional signature observed in stiff gel-embedded CD8$^+$ cells was at least in part driven by the mechano-regulation of key transcriptional regulators of T_{RM} cell differentiation, including Runx3, Hic1 and Klf2.

Stiffness imprints a T_{RM} cell-like phenotype retained in vivo

To assess whether the mechanosensitive transcriptome changes observed in activated CD8$^+$ T cells were stable, CD8$^+$ T cells were activated in media with CD3 + CD28 Ab, embedded in soft or stiff gels for 24 h and subsequently cultured in suspension for an additional 24 h (Fig. 6a). The differences in the expression of *Runx3*, *Klf2*, *Xcl1* and *Itga1* between soft and stiff gel-preconditioned CD8$^+$ T cells were retained in media at 24 h (Fig. 6b), suggesting that at least some mechanically induced gene expression changes were retained for a day. To assess whether mechanical preconditioning impacted CD8$^+$ T cell fate in vivo, we activated Thy1.1$^+$CD8$^+$ T cells in media with CD3 + CD28 Ab, preconditioned them for 24 h in soft or stiff collagen, and then injected them intradermally into the ears of B6.SJL CD45.1$^+$ recipient mice (Fig. 6c). We used intradermal injection, as downregulation of CD62L expression in stiff-preconditioned CD8$^+$ T cells precludes homing to secondary lymphoid organs after intravenous injection and most CD8$^+$ T cells drain from the skin to the (soft) ear-draining cervical LN (dLN) through lymphatic vessels in the absence of cognate antigen in the skin. At day 7 post transfer, while soft-gel-derived Thy1.1$^+$CD8$^+$ T cells in the dLN were mostly CD62L^{hi} T_{CM}-like, stiff gel-derived Thy1.1$^+$CD8$^+$ T cells in the dLN had increased percentages of CD62L^{lo}CD69$^+$ T_{RM}-like cells (CD103$^+$ and CD103$^-$) (Fig. 6d). We found a significant increase in both the percent and number of CD62L^{lo}Thy1.1$^+$CD8$^+$ T cells in the dLNs of mice transferred with stiff- compared to soft-preconditioned CD8$^+$ T cells (Fig. 6e), while the number of CD44$^+$CD62L^{hi}Thy1.1$^+$CD8$^+$ T_{CM}-like cells was similar between soft- and stiff-preconditioned transferred cells (Fig. 6f). Overall, stiff-preconditioned Thy1.1$^+$CD8$^+$ T cells were enriched in CD62L^{lo} T_{RM}-like cells by almost twofold compared to their soft-preconditioned counterparts in the dLN (Fig. 6f), and had a significantly higher proportion of CD69$^+$ or CD69$^+$CD103$^+$ T_{RM} cells compared to the soft-preconditioned Thy1.1$^+$CD8$^+$ T cells (Fig. 6g). By contrast, in the skin day 7 post transfer, all Thy1.1$^+$CD8$^+$ T cells were CD62L$^-$ in mice transferred with soft- or stiff-preconditioned CD8$^+$ T cells (Extended Data Fig. 8a), suggesting that skin tissue stiffness could still modulate cell phenotype. The number of stiff-preconditioned Thy1.1$^+$CD8$^+$CD62L^{lo} T_{RM}-like cells were slightly greater than soft-preconditioned T_{RM}-like cells in the skin (Extended Data Fig. 8a), possibly a result of greater retention.

To determine whether memory T cells located in stiffer non-lymphoid tissues displayed similar morphological features as activated CD8$^+$ T cells in stiff gels, we transferred spleen CD45.2$^+$CD8$^+$ T cells from nTnG-reporter mice activated in media with CD3 + CD28 Ab into CD45.1$^+$ mice infected with LCMV 4 days before transfer. We used confocal microscopy to detect transferred CD45.2$^+$ memory T cells in the spleen (soft) or lung and liver (stiff) at day 28 post transfer (Extended Data Fig. 8b). Extracted cell shape and nucleus shape parameters of transferred CD45.2$^+$ T cells across all three tissues indicated that cells separated in cell shape PCA space based on tissue (Fig. 6h), with lung and liver CD8$^+$ T cells having significantly greater cell perimeters and areas than those located in the spleen (Fig. 6i,j). Differences based on nuclear morphology were less pronounced (Extended Data Fig. 8c), with lung, but not liver CD45.2$^+$ T cell nuclei having significantly greater perimeters and areas than their splenic counterparts (Extended Data Fig. 8d). Thus, exposure of activated CD8$^+$ T cells to greater mechanical input led to increased differentiation of T_{RM}-like cells in vivo, and CD8$^+$ T_{RM} cells located in stiff tissues displayed morphology changes that may be mechanically driven.

Discussion

Our study revealed that activated CD8$^+$ T cells responded to mechanical cues in their microenvironment through changes in nuclear envelope composition, cell morphology and gene expression. Mechanosensing by activated CD8$^+$ T cells drove a core CD8$^+$ T_{RM} cell gene signature, leading to greater T_{RM} cell differentiation in vivo upon transfer of CD8$^+$ T cells preconditioned in stiff collagen. While the mechanosensor(s)

Fig. 6 | Stiffness imprints a T_{RM} cell-like phenotype retained in vivo. **a**, A schematic showing CD8$^+$ T cells were activated with CD3 + CD28 Ab in media for 3 days, preconditioned by embedding in soft (2 mg ml^{-1} atelo-bovine) or stiff (2 mg ml^{-1} telo-rat tail) collagen for 24 h, retrieved by digestion and then cultured in media for 24 h before analysis. **b**, Expression of *Runx3*, *Klf2*, *Xcl1* and *Itga1* measured by RT–qPCR in CD8$^+$ T cells (n = 4 mice, pooled from 2 independent experiments) cultured in soft and stiff gels as in **a**. Expression was normalized to a housekeeping gene and shown as FC relative to the mean of the ex-soft condition per gene. **c**, A schematic showing Thy1.1$^+$CD8$^+$ T cells were activated in media with CD3 + CD28 Ab for 3 days, embedded into soft or stiff collagen for 24 h, retrieved by digestion and adoptively transferred intradermally (i.d.) into the ears of WT CD45.1 mice, followed by isolation from the ear skin and dLN on day 11 (day 7 post transfer) and flow cytometry. **d**, Representative contour plots showing the phenotype of adoptively transferred Thy1.1$^+$CD8$^+$ T cells preconditioned in soft or stiff gels in the dLN of recipient mice at day 7 post transfer, as in **c**. **e**, The percent and number of CD62L^{lo} cells among adoptively transferred CD8$^+$ T cells preconditioned in soft or stiff gels in the dLN of recipient mice at day 7 post transfer, as in **c**. **f**, The number of T_{CM}-like cells and ratio of CD62L^{lo} to T_{CM} cell-like cells among transferred Thy1.1$^+$CD8$^+$ T cells preconditioned in soft or stiff gels in the dLN at 7 days postintradermal transfer as in **c**. The ratio is normalized to the mean ratio of adoptively transferred T cells preconditioned in soft collagen. **g**, The percentage of CD69$^+$CD103$^-$ and CD69$^+$CD103$^+$ CD62L^{lo} T_{RM}-like cells among Thy1.1$^+$CD8$^+$ T cells preconditioned in soft or stiff gels in the dLN at 7 days postintradermal transfer as in **c**. **h**, PCA of shape descriptors in memory CD45.2$^+$ T cells analyzed by confocal microscopy in the parenchyma of spleen (n = 150 cells), lung (n = 98 cells) and liver (n = 67 cells) of CD45.1 recipient mice infected with LCMV, transferred with CD3 + CD28 Ab-activated CD45.2$^+$nTnG$^+$CD8$^+$ T cells on day 4 post infection (n = 2 mice) and analyzed at day 28 post infection. The 95% CIs of s.e.m. are shown for each tissue. **i**, Summary of cell shape parameters (n = 2 mice) across tissues (spleen, lung and liver) that contributed most to the variance observed along the first principal component as in **h**. **j**, Example outlines of CD45.2$^+$ memory CD8$^+$ T cells from PCA as in **h**, colored by cell area. Cells were randomly sampled from the subpopulation of cells within PC1 ± 1 from respective tissue mean. Medians are shown in all quantification plots (**i**). In **e**–**g**, data are quantified from n = 9 mice; pooled from 2 independent experiments. Error bars are median ± min/max with box boundaries denoting 25th and 75th percentiles (**b**,**e**–**g**). Statistical tests: Mann–Whitney (**b**,**e**–**g**), ANOVA with Tukey's multiple comparisons test (**i**); all statistical tests were two sided; *P < 0.05, **P < 0.01, ***P < 0.001.

https://doi.org/10.1038/s41590-026-02581-9

responsible remains to be determined, we established that greater mechanical input led to the increased expression of Hic1 and Runx3, and decreased expression of KLF2—transcriptional regulators previously shown to be important in the differentiation of CD8$^+$ T_{RM} cells. Moreover, Hic1, Runx3 and KLF2 may not be the only T_{RM} cell-associated transcriptional regulators impacted by mechanical input. Given these findings, it is intriguing to speculate that at least part of the gene signature that defines the identity of CD8$^+$ T_{RM} cells is a cellular response to mechanical input, and that the core T_{RM} genes have a role in enabling CD8$^+$ T_{RM} cells to survive and remain motile in environments that are mechanically more challenging than lymphoid tissues.

Our data suggested that while YAP and TAZ may be involved in regulating some of the gene expression changes observed, they were not responsible for either the T_{RM} cell phenotype or the lamin A/C upregulation in CD8$^+$ T cells embedded in stiff gels. We also ruled out a role for integrin- or cPLA$_2$-mediated signaling, which in other settings translate mechanical forces into gene expression or cytoskeleton changes that impact cell migration[13,14,23], as well as myosin II-mediated cytoskeleton contractility or lamin A/C expression, in the induction of the T_{RM} cell-like transcriptome in stiff gel-embedded CD8$^+$ T cells. The extent of gene expression differences we observed in CD8$^+$ T cells between soft and stiff environments, at least some of which are stable after removal from the stiff gels, coupled with changes in lamin A/C expression and nuclear morphology, suggested that mechanical forces might ultimately lead to chromatin reorganization, as has been shown in other cell types[53]. Evidence from experiments injecting CD8$^+$ T cells preconditioned in soft or stiff collagen gels into the skin and examining their phenotype in the draining, much softer, LN environment suggested that mechanically induced changes were retained for at least a week. The mechanosensitive plasticity in T cells, and hence the

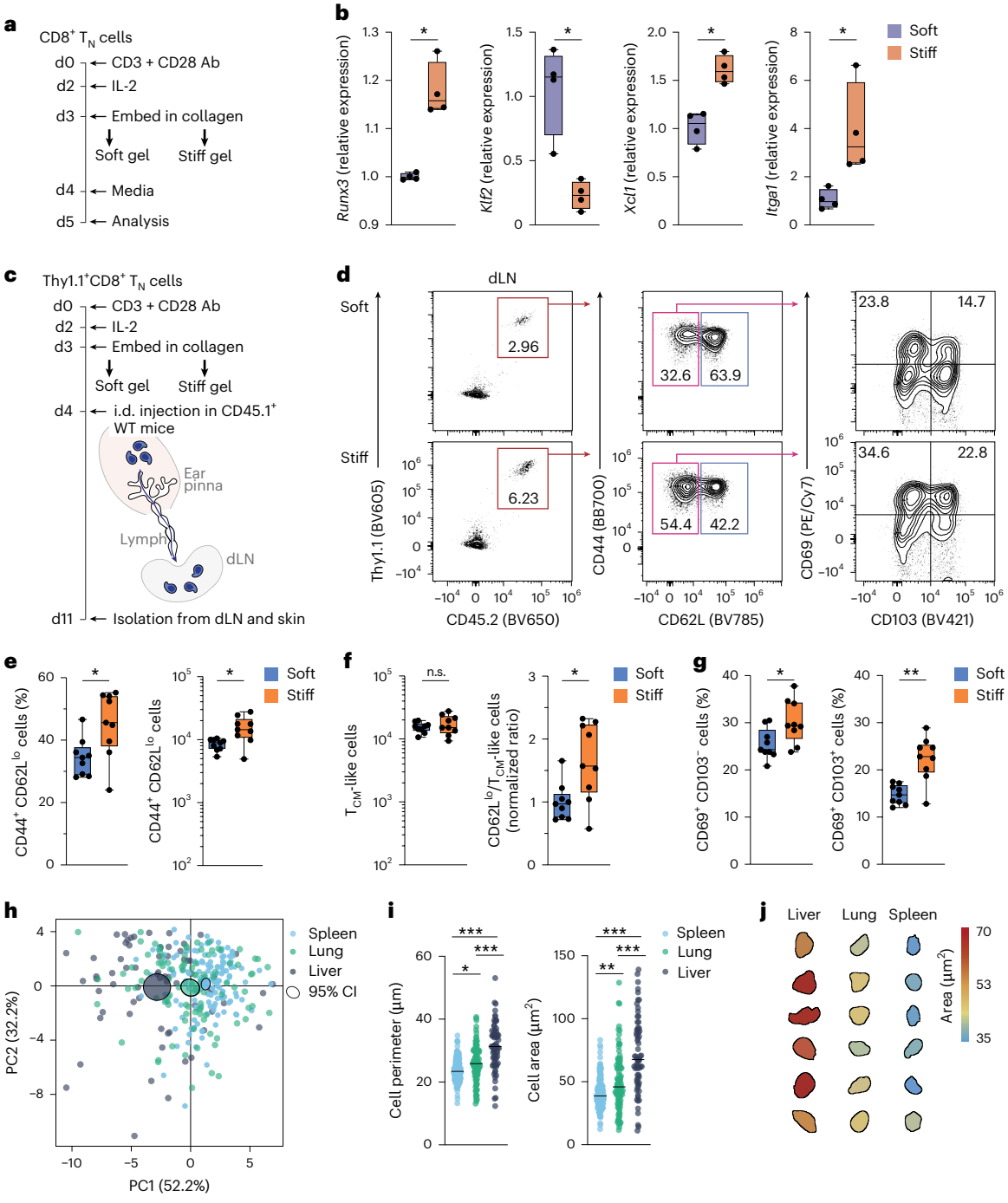

reversibility of mechanical force-instructed cell states, will be important to address. Activated T cells encounter changes in stiffness even before they traffic to peripheral tissues, as a result of the stiffening of lymphoid organs during infection[33]. Thus, it is possible that mechanosensing in lymphoid organs could have a role in preconditioning activated T cells for survival in tissues that exert greater mechanical forces. This would be in line with data suggesting that $CD8^+$ T_{RM} cell differentiation is initiated in lymphoid organs and further potentiated by tissue-specific signals[54,55]. Moreover, the overlap of stiffness-driven genes with genes downstream of TGFβ signaling may explain why TGFβ is important for $CD8^+$ T_{RM} cell differentiation in some tissues, while dispensable in others, despite the existence of a unifying T_{RM} cell gene program across all tissues[42].

The identification of a role for mechanical force sensing in $CD8^+$ T_{RM} cell differentiation may suggest novel therapeutic targets to impair $CD8^+$ T_{RM} cell maintenance in contexts where they are pathogenic, such as in autoimmune diseases, allergies or transplant rejection. In addition, modulating the trade-off between survival in the face of force-mediated DNA damage and the ability to remain motile in stiff microenvironments could be important in antitumor immunity. Determining whether molecular responses to increased external forces underlies why some immune cells can establish tissue residency, while others cannot, may eventually enable us to better tailor immune cell presence in distinct tissues in both health and disease.

Online content

Any methods, additional references, Nature Portfolio reporting summaries, source data, extended data, supplementary information, acknowledgements, peer review information; details of author contributions and competing interests; and statements of data and code availability are available at https://doi.org/10.1038/s41590-026-02581-9.

References

1. Mandl, J. N., Torabi-Parizi, P. & Germain, R. N. Visualization and dynamic analysis of host-pathogen interactions. *Curr. Opin. Immunol.* **29**, 8–15 (2014).
2. Farsakoglu, Y., McDonald, B. & Kaech, S. M. Motility matters: how $CD8^+$ T-cell trafficking influences effector and memory cell differentiation. *Cold Spring Harb. Perspect. Biol.* **13**, a038075 (2021).
3. Mueller, S. N. & Mackay, L. K. Tissue-resident memory T cells: local specialists in immune defence. *Nat. Rev. Immunol.* **16**, 79–89 (2016).
4. Charras, G. & Sahai, E. Physical influences of the extracellular environment on cell migration. *Nat. Rev. Mol. Cell Biol.* **15**, 813–824 (2014).
5. Guimarães, C. F., Gasperini, L., Marques, A. P. & Reis, R. L. The stiffness of living tissues and its implications for tissue engineering. *Nat. Rev. Mater.* **5**, 351–370 (2020).
6. Du, H. et al. Tuning immunity through tissue mechanotransduction. *Nat. Rev. Immunol.* **23**, 174–188 (2023).
7. Jeffreys, N., Brockman, J. M., Zhai, Y., Ingber, D. E. & Mooney, D. J. Mechanical forces amplify TCR mechanotransduction in T cell activation and function. *Appl. Phys. Rev.* **11**, 011304 (2024).
8. Cho, S. et al. Mechanosensing by the lamina protects against nuclear rupture, DNA damage, and cell-cycle arrest. *Dev. Cell* **49**, 920–935 (2019).
9. Swift, J. et al. Nuclear lamin-A scales with tissue stiffness and enhances matrix-directed differentiation. *Science* **341**, 1240104 (2013).
10. Harada, T. et al. Nuclear lamin stiffness is a barrier to 3D migration, but softness can limit survival. *J. Cell Biol.* **204**, 669–682 (2014).
11. Kalukula, Y., Stephens, A. D., Lammerding, J. & Gabriele, S. Mechanics and functional consequences of nuclear deformations. *Nat. Rev. Mol. Cell Biol.* **23**, 583–602 (2022).
12. Shen, C. et al. A Dock8-dependent mechanosensitive central actin pool maintains T cell shape and protects the nucleus during migration. *Sci. Immunol.* **10**, eadt9239 (2025).
13. Venturini, V. et al. The nucleus measures shape changes for cellular proprioception to control dynamic cell behavior. *Science* **370**, eaba2644 (2020).
14. Lomakin, A. J. et al. The nucleus acts as a ruler tailoring cell responses to spatial constraints. *Science* **370**, eaba2894 (2020).
15. Engler, A. J., Sen, S., Sweeney, H. L. & Discher, D. E. Matrix elasticity directs stem cell lineage specification. *Cell* **126**, 677–689 (2006).
16. Dupont, S. et al. Role of YAP/TAZ in mechanotransduction. *Nature* **474**, 179–183 (2011).
17. Reversat, A. et al. Cellular locomotion using environmental topography. *Nature* **582**, 582–585 (2020).
18. Wolf, K. et al. Physical limits of cell migration: control by ECM space and nuclear deformation and tuning by proteolysis and traction force. *J. Cell Biol.* **201**, 1069–1084 (2013).
19. Shayegan, M., Altindal, T., Kiefl, E. & Forde, N. R. Intact telopeptides enhance interactions between collagens. *Biophys. J.* **111**, 2404–2416 (2016).
20. Adu-Berchie, K. et al. Generation of functionally distinct T-cell populations by altering the viscoelasticity of their extracellular matrix. *Nat. Biomed. Eng.* **7**, 1374–1391 (2023).
21. Ruef, N. et al. Exocrine gland-resident memory $CD8^+$ T cells use mechanosensing for tissue surveillance. *Sci. Immunol.* **8**, eadd5724 (2023).
22. Ariotti, S. et al. Tissue-resident memory $CD8^+$ T cells continuously patrol skin epithelia to quickly recognize local antigen. *Proc. Natl Acad. Sci. USA* **109**, 19739–19744 (2012).
23. Saraswathibhatla, A., Indana, D. & Chaudhuri, O. Cell–extracellular matrix mechanotransduction in 3D. *Nat. Rev. Mol. Cell Biol.* **24**, 495–516 (2023).
24. Kirby, T. J. & Lammerding, J. Emerging views of the nucleus as a cellular mechanosensor. *Nat. Cell Biol.* **20**, 373–381 (2018).
25. Wang, N., Tytell, J. D. & Ingber, D. E. Mechanotransduction at a distance: mechanically coupling the extracellular matrix with the nucleus. *Nat. Rev. Mol. Cell Biol.* **10**, 75–82 (2009).
26. Martins, R. P., Finan, J. D., Guilak, F. & Lee, D. A. Mechanical regulation of nuclear structure and function. *Annu. Rev. Biomed. Eng.* **14**, 431–455 (2012).
27. Gilbert, H. T. J. et al. Nuclear decoupling is part of a rapid protein-level cellular response to high-intensity mechanical loading. *Nat. Commun.* **10**, 4149 (2019).
28. Gaspar, P. & Tapon, N. Sensing the local environment: actin architecture and Hippo signalling. *Curr. Opin. Cell Biol.* **31**, 74–83 (2014).
29. Wang, Y. et al. Comprehensive molecular characterization of the Hippo signaling pathway in cancer. *Cell Rep.* **25**, 1304–1317 (2018).
30. Raab, M. et al. ESCRT III repairs nuclear envelope ruptures during cell migration to limit DNA damage and cell death. *Science* **352**, 359–362 (2016).
31. Denais, C. M. et al. Nuclear envelope rupture and repair during cancer cell migration. *Science* **352**, 353–358 (2016).
32. Blackford, A. N. & Jackson, S. P. ATM, ATR, and DNA-PK: the trinity at the heart of the DNA damage response. *Mol. Cell* **66**, 801–817 (2017).
33. Meng, K. P., Majedi, F. S., Thauland, T. J. & Butte, M. J. Mechanosensing through YAP controls T cell activation and metabolism. *J. Exp. Med.* **217**, e20200053 (2020).
34. Mackay, L. K. et al. Hobit and Blimp1 instruct a universal transcriptional program of tissue residency in lymphocytes. *Science* **352**, 459–463 (2016).

35. Mackay, L. K. et al. The developmental pathway for CD103$^+$CD8$^+$ tissue-resident memory T cells of skin. *Nat. Immunol.* **14**, 1294–1301 (2013).
36. Behr, F. M. et al. Blimp-1 rather than Hobit drives the formation of tissue-resident memory CD8$^+$ T cells in the lungs. *Front. Immunol.* **10**, 400 (2019).
37. Crowl, J. T. et al. Tissue-resident memory CD8$^+$ T cells possess unique transcriptional, epigenetic and functional adaptations to different tissue environments. *Nat. Immunol.* **23**, 1121–1131 (2022).
38. Milner, J. J. et al. Runx3 programs CD8$^+$ T cell residency in non-lymphoid tissues and tumours. *Nature* **552**, 253–257 (2017).
39. Buquicchio, F. A. et al. Distinct epigenomic landscapes underlie tissue-specific memory T cell differentiation. *Immunity* **57**, 2202–2215 (2024).
40. Hombrink, P. et al. Programs for the persistence, vigilance and control of human CD8$^+$ lung-resident memory T cells. *Nat. Immunol.* **17**, 1467–1478 (2016).
41. Peng, C. et al. Engagement of the costimulatory molecule ICOS in tissues promotes establishment of CD8$^+$ tissue-resident memory T cells. *Immunity* **55**, 98–114 (2022).
42. Christo, S. N. et al. Discrete tissue microenvironments instruct diversity in resident memory T cell function and plasticity. *Nat. Immunol.* **22**, 1140–1151 (2021).
43. Derynck, R. & Zhang, Y. E. Smad-dependent and Smad-independent pathways in TGF-β family signalling. *Nature* **425**, 577–584 (2003).
44. Nath, A. P. et al. Comparative analysis reveals a role for TGF-β in shaping the residency-related transcriptional signature in tissue-resident memory CD8$^+$ T cells. *PLoS ONE* **14**, e0210495 (2019).
45. Obers, A. et al. Retinoic acid and TGF-β orchestrate organ-specific programs of tissue residency. *Immunity* **57**, 2615–2633 (2024).
46. Roy, N. H., MacKay, J. L., Robertson, T. F., Hammer, D. A. & Burkhardt, J. K. Crk adaptor proteins mediate actin-dependent T cell migration and mechanosensing induced by the integrin LFA-1. *Sci. Signal.* **11**, eaat3178 (2018).
47. Lammermann, T. et al. Rapid leukocyte migration by integrin-independent flowing and squeezing. *Nature* **453**, 51–55 (2008).
48. Fonseca, R. et al. Runx3 drives a CD8$^+$ T cell tissue residency program that is absent in CD4$^+$ T cells. *Nat. Immunol.* **23**, 1236–1245 (2022).
49. Skon, C. N. et al. Transcriptional downregulation of S1pr1 is required for the establishment of resident memory CD8$^+$ T cells. *Nat. Immunol.* **14**, 1285–1293 (2013).
50. Parmar, K. M. et al. Integration of flow-dependent endothelial phenotypes by Kruppel-like factor 2. *J. Clin. Invest.* **116**, 49–58 (2006).
51. Weinreich, M. A. et al. KLF2 transcription-factor deficiency in T cells results in unrestrained cytokine production and upregulation of bystander chemokine receptors. *Immunity* **31**, 122–130 (2009).
52. Chung, H. K. et al. Atlas-guided discovery of transcription factors for T cell programming. *Nature* **651**, 1077–1087 (2026).
53. Hunter, M. V. et al. Mechanical confinement governs phenotypic plasticity in melanoma. *Nature* **647**, 517–527 (2025).
54. Kok, L., Masopust, D. & Schumacher, T. N. The precursors of CD8$^+$ tissue resident memory T cells: from lymphoid organs to infected tissues. *Nat. Rev. Immunol.* **22**, 283–293 (2022).
55. Mani, V. et al. Migratory DCs activate TGF-β to precondition naive CD8$^+$ T cells for tissue-resident memory fate. *Science* **366**, eaav5728 (2019).
56. Wherry, E. J. et al. Molecular signature of CD8$^+$ T cell exhaustion during chronic viral infection. *Immunity* **27**, 670–684 (2007).

Methods

Mice

C57BL/6J (JAX 000664), B6.Thy1.1 (JAX 000406), B6.CD45.1 (JAX 033076) and vav-cre (JAX 035670[57]) mice were purchased from The Jackson Laboratory. LifeAct-GFP reporter mice[58] (shared by J. Burkhardt, University of Pennsylvania) were crossed in-house with nTnG reporter mice (JAX 023537)[59]. $YAP^{fl/fl}/TAZ^{fl/fl}$ mice[60] were shared by A. Gregorieff (McGill); $Thy1.1^{+}$ P14 TCR transgenic mice[61] by H. Melichar (McGill). $Lmna^{fl/fl}$ mice[62] were shared by J. Lammerding (Cornell University) and crossed to vav-cre mice in-house. All mice were bred and housed under SPF conditions with a 12 h/12 h light/dark cycle at an ambient temperature of 18–24 °C and a humidity range of 30–70% in the CMARC animal facility (McGill), in accordance with the Guide for the Care and Use of Laboratory Animals, with exception of KLF2–GFP reporter[51] mice, which were bred at the University of Minnesota in the lab of S. Jameson and spleens shipped on ice to Montreal. All mice were on a C57BL/6J background and used for experiments at 6–12 weeks of age. Both male and female mice were used and sex matched where applicable. Randomization and blinding were not used. The sample size was determined by power analysis and prior experience. No data points were excluded from the analyses. Experimental procedures were all approved by the McGill University Facility Animal Care Committee (protocol no. MCGL-7570).

Human samples

Human blood samples were obtained by venipuncture at the Center for Innovative Medicine, Research Institute of the McGill University Health Center. Informed consent was obtained from all volunteers. Participants were male and female, healthy, aged 29–38 years old. This study was approved by the McGill University Health Center Research Ethics Board (protocol no. 2023-8829).

Buffers, culture media and centrifugation settings

Reagents were purchased from Wisent unless otherwise indicated.

Complete media: RPMI 1640 supplemented with 10% heat-inactivated fetal bovine serum (FBS), 2 mM L-glutamine, 100 U ml^{-1} penicillin, 100 ng ml^{-1} streptomycin, 1 mM sodium pyruvate, 10 mM HEPES, 1% nonessential amino acids (NEAA) and 5 µM 2-mercaptoethanol (Gibco).

StemCell isolation buffer: PBS (without Ca^{2+} and Mg^{2+}) supplemented with 2% FBS and 1 mM EDTA (Gibco).

Concentrated RPMI for collagen gel: for 1 ml; 620 µl RPMI 1640 10× (Sigma) supplemented with 165 µl sodium bicarbonate 7.5% solution (Gibco), 155 µl HEPES 1 M and 62 µL L-glutamine 200 mM. pH was adjusted to 7.4 using NaOH 1 N (Sigma).

FACS buffer: PBS (without Ca^{2+} and Mg^{2+}) supplemented with 2% FBS and 5 mM EDTA (Gibco).

Digestion buffer: RPMI 1640 supplemented with 0.25 mg ml^{-1} Liberase TL (Roche) and 50 U ml^{-1} DNAse I (Sigma).

Comet assay lysis buffer: 2.5 M NaCl, 10 mM Tris, 100 mM EDTA and 1% Triton X-100 (pH 10).

Comet assay electrophoresis alkaline buffer: 300 mM NaOH and 1 mM EDTA (pH >13).

Comet assay neutralization buffer: 400 mM Tris (pH 7.5).

Centrifugation settings: unless otherwise specified, cells were centrifuged at 300*g* for 5 min at 4 °C.

$CD8^{+}$ T cell isolation for activation and expansion

Murine $CD8^{+}$ T cell isolation. Spleen and LN (inguinal, axillary, brachial, superficial cervical and mesenteric) were collected and crushed through a 70-µm strainer in StemCell buffer. After centrifugation, red blood cells were lysed in 3 ml ACK Lysing buffer (Gibco) for 1 min, and cells were washed in StemCell buffer. $CD8^{+}$ T cells were isolated using EasySep Mouse Total $CD8^{+}$ T Cell Isolation Kit (StemCell) following the manufacturer's protocol with an additional magnet separation step, then washed in complete media (for activation) or PBS (for adoptive transfer). To generate inducible knockout of Talin or double knockout of YAP and TAZ, $CD8^{+}$ T cells were incubated with 2 µM TAT-CRE Recombinase (Sigma) for 1 h at 37 °C to excise the transgenes flanked by loxP sites before CD3 + CD28 Ab activation.

Murine $CD8^{+}$ T cell activation. Flat-bottom 96-well plates were coated with 3 µg ml^{-1} Ultra-LEAF Purified anti-mouse CD3ε (145-2C11, BioLegend) for 2 h at 37 °C or overnight at 4 °C, then washed with PBS. Isolated $CD8^{+}$ T cells were resuspended at 2.5×10^{6} cells ml^{-1} in complete media and supplemented with 2 µg ml^{-1} Ultra-LEAF purified anti-mouse CD28 (37.51, BioLegend). Then 200 µl of 5×10^{5} cells were added per well. After 2 days at 37 °C, 5% CO_2, cells were pooled, centrifuged, resuspended at 10^{6} cells ml^{-1} in complete media with 20 ng ml^{-1} recombinant mouse IL-2 (BioLegend), and expanded in T75 flasks at 37 °C, 5% CO_2. Cells were loaded in collagen gels on day 3.

P14 $CD8^{+}$ T cell activation. Naive $CD8^{+}$ T cells from $Thy1.1^{+}$ P14 $TCR\alpha^{-/-}$ transgenic mice were isolated using the EasySep Mouse Total T Cell Isolation Kit (StemCell). Splenocytes from $CD45.1^{+}$ mice were treated with mitomycin C (50 µg ml^{-1}; Sigma) for 25 min at 37 °C, washed three times in RPMI with 1% FBS, pulsed with 4 µM GP33–41 (Anaspec) peptide for 2 h at 37 °C and washed twice. P14 cells and peptide-pulsed splenocytes were co-cultured at a 1:10 ratio (1.8×10^{5} T cells and 1.8×10^{6} splenocytes per well) in 1 ml complete media in 48-well plates at 37 °C, 5% CO_2. After 2 days, cells were pooled, centrifuged and resuspended at 10^{6} cells ml^{-1} in complete media with 20 ng ml^{-1} recombinant mouse IL-2 (BioLegend), expanded in T25 flasks and used on day 3.

Human $CD8^{+}$ T cell activation. PBMCs were isolated from whole blood using Ficoll-Paque PLUS Density Gradient Media (Cytiva) following the manufacturer's instructions. $CD8^{+}$ T cells were purified using EasySep Human $CD8^{+}$ T Cell Isolation Kit (StemCell), washed and resuspended at 10^{6} cells ml^{-1} in complete media supplemented with 25 µl ml^{-1} of ImmunoCult Human CD3/CD28 T Cell Activator (StemCell) and 20 ng ml^{-1} recombinant human IL-2 (BioLegend). Cells were plated in 200 µl in flat-bottom 96-well plates at 5×10^{5} cells $well^{-1}$ and incubated at 37 °C, 5% CO_2. On days 3 and 6 post activation, cells were supplemented with fresh media and IL-2. Cells were loaded in collagen gels at 8 or 15 days post activation.

Collagen gels

Cell loading. Activated $CD8^{+}$ T cells were washed, resuspended at 1.6×10^{7} cells ml^{-1} in FBS. The atelo-bovine collagen gels (Nutragen Solution, Advanced Biomatrix), telo-bovine collagen (TeloCol Solution, Advanced Biomatrix) and rat tail telo-collagen (RatCol Solution, Advanced Biomatrix) were prepared as follows in 12-well plates on ice. Atelo-bovine: 366 µl sterile molecular grade water, 33.3 µl neutralization buffer (supplied by manufacturer), 333 µl Nutragen Solution, 142 µl concentrated RPMI and 125 µl cell suspension (2×10^{6} cells). Telo-bovine: 366 µl sterile molecular grade water, 33.3 µl neutralization buffer, 333 µl TeloCol Solution, 142 µl concentrated RPMI and 125 µl cell suspension. Telo-rat tail: 185 µl sterile molecular grade water, 50 µl neutralization buffer, 500 µl RatCol Solution, 142 µl concentrated RPMI and 125 µl cell suspension. Wells were gently mixed, gels polymerized at 37 °C, 5% CO_2, and incubated for 24 h.

Cell treatment in collagen gels. For in-gel treatment of cells, drugs were mixed in concentrated RPMI and incorporated into gels. Final concentrations: α-TGFβ (Biolegend), 10 µg ml^{-1}; recombinant (rm) TGFβ (Biolegend), 3 nM (ref. 44); DNA repair inhibitor NU7441 (Cayman Chemical Company), 2 µM; $cPLA_2$ inhibitor AACOCF3 (VWR), 25 µM; YAP inhibitor verteporfin (Tocris), 125 nM; Myosin II inhibitor (*S*)-4′-nitro-blebbistatin (Cayman Chemical Company), 20 µM; F-actin polymerization inhibitor latrunculin B (Cayman Chemical Company), 0.5 µM.

Cell recovery. Each collagen gel was digested with 100 mg ml^{-1} collagenase D (Sigma) at 37 °C with shaking for 30 min. Cells were resuspended in FACS buffer for flow cytometry or lysis buffer for RNA extraction.

Ex vivo T cell restimulation. $CD8^+$ T cells were recovered from gels after 24 h, resuspended in complete media and stimulated with 10 ng ml^{-1} phorbol 12-myristate 13-acetate (PMA; Sigma) and 1 µg ml^{-1} ionomycin (Sigma) in the presence of brefeldin A (5 µg ml^{-1}; BioLegend) for 4 h at 37 °C, 5% CO_2. An unstimulated control was incubated with brefeldin A only. Following restimulation, cells were washed and processed for flow cytometry.

Generation of ex-soft and ex-stiff cells. $CD8^+$ T cells were recovered from collagen gels and resuspended at 10^6 cells ml^{-1} in complete media supplemented with 20 ng ml^{-1} recombinant mouse IL-2 (BioLegend). Cells were rested for 24 h in T75 flasks at 37 °C, 5% CO_2, to generate ex-soft and ex-stiff T cell cultures.

ELISA of collagen gels. Active TGFβ levels were quantified using the LEGEND MAX Free Active TGFβ1 ELISA Kit with precoated plates (BioLegend), according to the manufacturer's instructions. Retinoic acid levels were quantified using the Mouse Retinoic Acid ELISA Kit (AFG Scientific) according to the manufacturer's instructions. All inhibitors/reagents and assay kits used are listed in Supplementary Table 4.

Intradermal cell transfer and tissue processing

Intradermal injection. $CD8^+$ T cells were isolated from collagen gels after 24 h as described, with the following modification: cells were passed through a prerinsed LS column (Miltenyi) right after digestion to remove dead cells and debris, and then centrifuged at 100*g*. The isolated $CD8^+$ T cells were counted and resuspended at 1.5×10^8 cells ml^{-1} in PBS and kept at 4 °C until injected. Mice were anesthetized using isoflurane, and their ears taped on a conical tube. Then 10 µl of cell suspension (1.5×10^6 cells) was intradermally transferred into each ear using a Hamilton Syringe (Sigma). Mice were euthanized 7 days post injection.

Tissue processing. Ears and ear-draining LNs were collected in cold RPMI on ice. Ventral and dorsal ear sheets were separated and digested in 1 ml digestion buffer for 45 min at 37 °C, with shaking (200 rpm); digestion was stopped with 500 µl FACS buffer. Ears were crushed through a 100-µm strainer, centrifuged, resuspended in 1 ml of FACS buffer and filtered through a 60-µm nylon mesh. dLN were crushed in microtubes using pellet pestles (Fisher Scientific), centrifuged, resuspended in 1 ml of FACS buffer and filtered through a 60-µm nylon mesh. Suspensions were kept on ice for flow cytometry analysis.

Flow cytometry

Staining. Cells (2×10^6 cells $well^{-1}$) were plated in 96-well V-bottom plates. Extracellular staining of cells was performed with fluorescently conjugated antibodies diluted in FACS buffer with a viability dye and either TruStain FcX (anti-mouse CD16/32 antibody, BioLegend) or Human TruStain FcX (Fc Receptor Blocking Solution, BioLegend) for 20 min at 4 °C. For intracellular staining, cells were washed in PBS, fixed in 2% paraformaldehyde (PFA) for 30 min at 4 °C, washed in FACS buffer and stained with antibodies in FACS buffer supplemented with 0.3% Triton X-100 for 60 min at 4 °C. Cells were washed, resuspended in 200 µl FACS buffer and filtered over a 60-µm nylon mesh. All antibodies and viability dyes used are listed in Supplementary Table 4.

Acquisition. Samples were acquired on a LSRFortessa flow analyzer (BD Biosciences) or an Aurora spectral flow analyzer (Cytek). Data were analyzed with FlowJo software (BD Biosciences).

RNA-seq and RT–qPCR

RNA extraction was performed using the PureLink RNA Mini Kit (Invitrogen) following the manufacturer's instructions. Typically, 2×10^6 $CD8^+$ T cells were lysed when activated, 5×10^6 when naive. RNA concentration was quantified by a NanoDrop (Thermo Scientific). Isolated RNA was stored at −80 °C or converted to cDNA.

Bulk RNA-seq. Purified RNA was provided to the IRCM sequencing core facility (Quebec, Canada). RNA quality control was performed by Pico assay with a bioanalyzer (Agilent). RNA-seq libraries were prepared from 150 ng RNA per condition using the following kits: RiboCop rRNA Depletion Kit HMR (Lexogen), KAPA RNA HyperPrep Kit (Roche) and TruSeq DNA UDI 96 Indexes (Illumina). Libraries were sequenced on a NovaSeq 6000 System (Illumina) using a Flow Cell S2 (Illumina) and a paired-end run. At least 60 million paired-end reads were generated per sample. Reads were quality checked using FastQC and MultiQC and mapped to the GRCm38/mm10 *Mus musculus* genome using HISAT2. Alignment quality check was performed using Samtools Flagstat, FastQC, Picard Tools and MultiQC. Sequencing reads overlapping exons were counted using featureCounts. Differential gene expression analysis was performed using EdgeR (R Project[63]), filtering out low-expression genes using the filterByExpr function, and normalizing the read counts (calcNormFactors function). *P* values were corrected using the Benjamini–Hochberg method and only genes with an false discovery rate (FDR) <0.01 were considered statistically significant. No fold change (FC) threshold was set unless stated.

Two-step RT–qPCR. Reverse transcription of purified RNA was performed using the High-Capacity cDNA Reverse Transcription Kit (Applied Biosystems) following the manufacturer's protocol using 500 ng RNA per 20 µl mix. The obtained cDNA was diluted five times with molecular grade water and stored at −20 °C. qPCR was performed on a StepOnePlus Real-Time PCR System (Applied Biosystems) using 2 µl of diluted cDNA per well (10 ng) as template, the primers listed in Supplementary Table 5 and TaqMan Fast Advanced Master Mix (Applied Biosystems).

RNA-seq analyses

PCA and correlation matrices were built from CPM values using the prcomp function and the cor function (respectively) from the R statistical computing package, and ggplot2 and factoextra packages for data visualization[63]. Volcano plots were generated using the ggplot2 package. Heat maps were built from CPM values using pheatmap. CPM values were centered and scaled in the row direction. GSEAs were performed as previously described using sets defined by the Molecular Signatures Database (MSigDB) and default settings (including permutation by phenotype)[64]. T_{RM} cell core gene sets were curated from ref. 35 (Fig. 4c) and are listed in Supplementary Table 2. T effector gene sets were from ref. 56 (Fig. 4f) and ref. 65 (Extended Data Fig. 4a). TGFβ-regulated genes in T cells were from ref. 44 (Extended Data Fig. 5d,e). Details on all other GSEA datasets are provided in figure legends. GO analysis was performed using Metascape[66]. Only genes that were significantly upregulated in the stiff condition (FDR <0.01 and FC >2) were included. Enriched clusters identified with less than 50 genes were filtered out.

Collagen gels and tissue stiffness measurements

Nanoindentation. Collagen gels were prepared and loaded in eight-well Lab-Tek chambers (600 µl $well^{-1}$). Before measurement, PBS was added on top of the gels. Organs were collected, cleaned of fat and embedded in agarose gels made of 5% agarose in complete RPMI. All organs were sectioned using a vibratome, except for lung tissues, which were not sectioned. Agarose pads with tissue sections were glued onto Petri dishes using Vetbond (3 M) and immersed in PBS. Stiffness was measured using a displacement-controlled nanoindenter (Piuma, Optics11 Life) coupled with a glass spherical probe with a radius of

25 µm and a spring constant of 0.025 N m^{-1} (for collagen gels, LN and spleens) or a glass spherical probe with a radius of 25 µm and a spring constant of 0.5 N m^{-1} (for all other organs) (Optics11 Life). Cantilever calibration was performed using a glass Petri dish before each series of measurements. Each collagen gel was indented at least nine times and at least 100 µm apart; each organ was indented nine times in a 3 × 3 matrix 80 µm apart. At least two biological repeats were performed per organ. The indentation process consisted of a loading phase for 2 s at 15 µm indentation depth, which was held for 1 s, and then an unloading phase for 2 s. The Young's elastic modulus was calculated from single indentation measurements using the 'Hertzian contact' model setting. Organ or collagen stiffness was plotted as the mean value of all the measurements performed in each scan per mouse.

Rheology of collagen gels. Shear rheological characterization of the collagen gels was performed on modular compact rheometer (MCR-302, Anton Paar) set with a cone-and-plate geometry (CP-25, Anton Paar). For each measurement, 200 µl of ice-cold unpolymerized collagen mixture was loaded on a Pelletier plate set to 4 °C before lowering the cone-plate spindle to final position. Excess gel was removed, mineral oil was added to prevent dehydration and the Pelletier plate was set to 37 °C, which sets the beginning of the measurements. An oscillatory time-sweep (1% strain, 1 Hz) was conducted at 37 °C for 15 min to measure the storage modulus (G′), loss modulus (G″) and the loss angle. At the end of the isothermal gelation, a shear stress relaxation test was performed applying 20% shear strain within 1 s and maintaining the 20% strain while recording changes in shear stress for 2 min at 37 °C.

LCMV infection

Mice were infected intraperitoneally with 2×10^5 plaque-forming units of LCMV-Armstrong, originally provided by J. Harty (University of Iowa). For nanoindentation measurements, spleens were collected 7 days post infection. To quantify memory T cell morphologies in tissues, $CD8^+$ T cells were isolated from $CD45.2^+$ LifeAct-nTnG mice, activated in vitro with CD3 + CD28 Ab as described, and expanded for 4 days; then 3×10^7 cells were adoptively intravenously transferred into $CD45.1^+$ recipients. Recipients were infected with LCMV 4 days before adoptive transfer. At 28 days post infection, lung, liver and spleen were collected and immediately placed into PLP buffer (0.05 M phosphate buffer, 0.1 M L-lysine, pH 7.4, 2 mg ml^{-1} NaIO4 and 10 mg ml^{-1} PFA) for fixation. Organs were fixed overnight in PLP buffer followed by dehydration in 30% sucrose overnight. Tissues were frozen in Tissue-Tek O.C.T compound (VWR) and stored at −80 °C until sectioned into 30-µm slices with a cryostat (Epredia CryoStar NX50) set to −20 °C. Sections were incubated with blocking buffer (0.1 M Tris, 1% FBS, 0.3% Triton X-100, 1% gelatin from cold water fish scales) for 1 h then stained with a primary rabbit α-CD31 antibody (Cell Signaling Technology) overnight, followed by a goat α-rabbit AF514 secondary antibody (Invitrogen). Tissue sections were incubated in blocking buffer with 1% rat serum for 1 h and subsequently stained with α-CD45.2 AF647 (Invitrogen) and DAPI (Sigma). Slides were mounted with ProLong Gold Antifade Reagent (Invitrogen, P36930) and kept at 4 °C. Confocal images were acquired with a Zeiss LSM880 using a 40× plan-apochromat DIC oil immersion, NA 1.3 objective.

Imaging of cell migration in collagen gels

Live-cell imaging. Atelo-bovine collagen and rat tail telo-collagen was fluorescently labeled with AF647 as described[12,67] and polymerized in 150-µl gels that were transferred to custom-made 3D chambers on glass slides. T cells used for live imaging were isolated from LifeAct-nTnG mice for activation. Gels were imaged on a Zeiss LSM880 confocal microscope equipped with a Plan-Apochromat 20×/1.0 NA water immersion objective. *Z* stacks of 60 planes spaced by 2 µm were acquired every minute for 30 min. Positional coordinates of cells were extracted using the Surfaces tool of Imaris (v.10.0). The R package celltrackR (v.1.2.0) was used to plot cell tracks and compute migratory speeds from movies of cells migrating through collagen gels[68].

Imaging of fixed gels. Collagen gels (50 µl) were transferred to 96-well, black, optically clear flat-bottom, tissue-culture treated plates (PerkinElmer). All reagents used for staining were slowly added on top of the gels and removed by inverting the plate. The staining protocol was as follows: fixation with 4% PFA for 1 h at 37 °C, PFA quenching with 0.15 M glycine in TBS for 1 h at room temperature, cell permeabilization with 0.5% Triton X-100 and 5% rat serum in TBS for 2 h at room temperature, cell staining overnight at 4 °C (directly conjugated antibodies) or 4 h at room temperature (phalloidin and nuclear dyes), mounting by adding 50 µl of Prolong Gold antifade reagent (Cell Signaling Technology), with three washes, 20 min each with TBS or 0.1% Tween in TBS between each step. Collagen gels were imaged with an inverted spinning-disk confocal microscope (Opera Phenix HCS, PerkinElmer) equipped with a 40×, NA 1.1 water objective. Typically, images from 300 *z* planes spaced by 2 µm were collected.

For higher-resolution imaging, activated $CD8^+$ T cells were resuspended at 1.2×10^8 cells ml^{-1} in FBS, mixed with collagen master mix in a Lab-Tek II Chamber Slide (Thermo Scientific, 154534PK) and incubated for 24 h at 37 °C, 5% CO_2. Gels were fixed with prewarmed 4% PFA for 30 min at room temperature, washed three times with PBS for 5 min, permeabilized with 0.2% Triton X-100 in PBS for 30 min at room temperature and blocked in 10% goat serum and 1% IgG-free BSA in PBS for 1 h at 4 °C. Between steps, gels were washed with 0.05% Tween-20 in PBS (PBST) three to five times for 5 min each. Sequential overnight staining at 4 °C was performed (exception Lamin A/C, Cell Signaling Technologies, 41357S; 24 h incubation) on a rocking shaker in the dark by incubating the gels in antibody diluent (2% IgG-free BSA and 0.1% Triton X-100 in PBS) containing a single antibody, followed by washes with 0.05% PBST between stains. Gels were stained with phalloidin-AF555 (Invitrogen) and Hoechst 34580 (0.5 µg ml^{-1}, BD Biosciences) for 1 h at room temperature in the dark. Gels were mounted on 35-mm glass-bottom dishes (Ibidi) and imaged within 24 h using a Leica Stellaris-8 automated inverted confocal microscope, equipped with a plan-apochromat 100×/1.40 oil STED White objective. *Z* stacks were acquired with 0.5-µm axial steps.

Under-agarose migration assay

Assays were performed as in ref. 12. KLF2–GFP T cells were labeled with Hoechst 34580 (0.5 µg ml^{-1}; BD Biosciences) in PBS for 5 min at 37 °C, washed with PBS and resuspended in phenol red-free complete media (10^7 cells ml^{-1}) for loading into the first access port. CCL19 (2 µg ml^{-1}) was loaded into the second port. Cells migrated at 37 °C, 5% CO_2 for 3 h before imaging. To maintain viability, half the access port volume was replaced with phenol red-free complete media supplemented with rIL-2 (20 ng ml^{-1}) at 5 h and 20 h post-loading. For unconfined migration, KLF2–GFP T cells (10^7 cells ml^{-1} in phenol red-free cRPMI) were seeded on fibronectin-10 (Sigma)-coated 35-mm glass-bottom dishes (prepared as above), with rIL-2 (20 ng ml^{-1}). Live cells were imaged at 3 h, 6 h and 24 h post-loading using a Zeiss Axio Observer Fully Automated Inverted Microscope (63× plan-apochromat, NA 1.40, oil, DIC objective) with a humidified stage top incubator (37 °C, 5% CO_2).

Shape analysis

Processing of collagen gel images. Image stacks were volume rendered in Imaris (Bitplane) and cells and nuclei were segmented using the Surfaces model. For shape analysis purposes we excluded cells that were not entirely captured, cell debris, cells forming doublets (diving cells and physical doublets), cells dying (identified by blebbing morphology), tdTomato reporter leakage into the cytoplasm indicating nuclear envelope rupture, absence of phalloidin signal

(cytoplasm) or the absence of tdTomato signal (nucleus). The surfaces obtained for cells and nuclei were used to create a mask of viable single cells and nuclei. Three-dimensional masked images were converted to two-dimensional images by maximum intensity *z* projection and binarized in Fiji using the threshold function[69].

Processing of tissue confocal images. Confocal *z* stacks were background subtracted in Fiji and segmented using the cellpose cyto3 model[70,71]. Slice-by-slice (two-dimensional) segmentation was performed with three-dimensional stitching using a stitch threshold (IoU) of 0.4. Cell masks and intensity images were linked using custom Fiji macros (provided by J. Ryan, Advanced BioImaging Facility) for shape parameter extraction, requiring cell appearance in ≥3 slices to exclude debris. For nuclear analysis, a >100-pixel intensity threshold removed nonspecific background objects. Only cells in the tissue parenchyma (determined by CD31 vascular staining) were included in the analysis.

PCA plot of shape descriptors. Shape descriptors were obtained from the two-dimensional binary images using both the Analyze Particle function in Fiji (parameters: Feret, MinFeret, AR, Round and Solidity) and the Analyze Regions from the MorphoLibJ library (parameters: Area, Perimeter, Circularity, Ellipse.Radius1, Ellipse.Radius2, Ellipse.Elong, ConvexArea, Convexity, OBox.Length, OBox.Width, GeodesicDiameter, Tortuosity, InscrDisc.Radius, AverageThickness and GeodesicElongation). PCA was performed using prcomp (R stats package) and visualized with factoextra[63].

Alkaline comet assay

Glass slides were precoated by dipping in 1% normal melting point agarose (Invitrogen) in distilled water and dried overnight at room temperature. $CD8^+$ T cells isolated from soft and stiff gels (2×10^6 cells ml^{-1} in PBS, 50 µl) were mixed with 450 µl of 1% low melting point agarose. Drops (50 µl) of cell–agarose mixture were placed onto precoated slides, covered with coverslips and refrigerated for 15 min. After coverslip removal, slides were immersed in comet assay lysis buffer for 2 h at 4 °C in the dark, washed 3× 5 min each in cold electrophoresis buffer and incubated in the same buffer for 20 min in the electrophoresis chamber. Alkaline electrophoresis was run at a 1 V cm^{-1} for 30 min at 4 °C in the dark. The current was adjusted to 300 mA as needed. Slides were washed once in neutralization buffer (5 min), twice in distilled water (5 min each) and once in 70% EtOH (5 min) at room temperature, then air dried. DNA was stained with SYBR Gold (Invitrogen, 1:10,000 in TE) for 20 min at room temperature in the dark, washed in distilled water and imaged using an epifluorescence microscope with a 10× objective.

Statistical analyses

Data are reported as scatter plots or box plots (center lines, medians; boxes, quartiles; whiskers, min to max) with all data points shown. Sample sizes, numbers of independent experiments and summary statistics are specified in figure legends. Nonparametric statistical tests were used throughout. Statistical comparisons were performed in Prism (GraphPad); tests are indicated in figure legends. Significance was defined by $P < 0.05$ and reported as $*0.01 < P < 0.05$, $**0.001 < P \leq 0.01$ or $***P \leq 0.001$.

Reporting summary

Further information on research design is available in the Nature Portfolio Reporting Summary linked to this article.

Data availability

Further information and requests for resources and source data should be directed to and will be fulfilled by the lead contact, J.N.M. RNA-seq data can be accessed in NCBI Gene Expression Omnibus (accession no. GSE278556). This study did not generate unique reagents.

References

57. Stadtfeld, M. & Graf, T. Assessing the role of hematopoietic plasticity for endothelial and hepatocyte development by non-invasive lineage tracing. *Development* **132**, 203–213 (2005).
58. Riedl, J. et al. Lifeact mice for studying F-actin dynamics. *Nat. Methods* **7**, 168–169 (2010).
59. Prigge, J. R. et al. Nuclear double-fluorescent reporter for in vivo and ex vivo analyses of biological transitions in mouse nuclei. *Mamm. Genome* **24**, 389–399 (2013).
60. Reginensi, A. et al. Yap- and Cdc42-dependent nephrogenesis and morphogenesis during mouse kidney development. *PLoS Genet.* **9**, e1003380 (2013).
61. Pircher, H. et al. Molecular analysis of the antigen receptor of virus-specific cytotoxic T cells and identification of a new V alpha family. *Eur. J. Immunol.* **17**, 1843–1846 (1987).
62. Sullivan, T. et al. Loss of A-type lamin expression compromises nuclear envelope integrity leading to muscular dystrophy. *J. Cell Biol.* **147**, 913–920 (1999).
63. R Core Team *R: A Language and Environment for Statistical Computing* (R Foundation for Statistical Computing, 2025); https://www.R-project.org/
64. Subramanian, A. et al. Gene set enrichment analysis: a knowledge-based approach for interpreting genome-wide expression profiles. *Proc. Natl Acad. Sci. USA* **102**, 15545–15550 (2005).
65. Luckey, C. J. et al. Memory T and memory B cells share a transcriptional program of self-renewal with long-term hematopoietic stem cells. *Proc. Natl Acad. Sci. USA* **103**, 3304–3309 (2006).
66. Zhou, Y. et al. Metascape provides a biologist-oriented resource for the analysis of systems-level datasets. *Nat. Commun.* **10**, 1523 (2019).
67. Doyle, A. D. Fluorescent labeling of rat-tail collagen for 3D fluorescence imaging. *Bio Protoc.* **8**, e2919 (2018).
68. Wortel, I. M. N. et al. CelltrackR: an R package for fast and flexible analysis of immune cell migration data. *Immunoinformatics* **1–2**, 100003 (2021).
69. Schindelin, J. et al. Fiji: an open-source platform for biological-image analysis. *Nat. Methods* **9**, 676–682 (2012).
70. Stringer, C., Wang, T., Michaelos, M. & Pachitariu, M. Cellpose: a generalist algorithm for cellular segmentation. *Nat. Methods* **18**, 100–106 (2021).
71. Stringer, C. & Pachitariu, M. Cellpose3: one-click image restoration for improved cellular segmentation. *Nat. Methods* **22**, 592–599 (2025).

Acknowledgements

We thank R. Germain (NIH) and H. Melichar (McGill), as well as the members of the Mandl lab for their helpful feedback on the paper. We thank G. Perreault, K. Prud'homme and the staff from the Comparative Medicine and Animal Resources Centre (CMARC) for the maintenance of our mouse colony; C. Stegen and J. Leconte from the McGill University flow cytometry core facility; and J. Ryan and the staff of the McGill University Advanced BioImaging Facility (ABIF, RRID: SCR_017697). O. Neyret and S. Boissel from the Molecular Biology and Functional Genomics Core Facility located at the Institut de Recherches Cliniques de Montréal (IRCM) performed the library prep for the RNA-seq dataset used in the study. Computational analyses were enabled in part by support provided by Calcul Québec and Compute Canada.

Author contributions

J.N.M. conceived of and supervised the project. J.N.M., J.P., M.M. and A.R.M. designed the research. Experiments were performed and analyzed by J.P., M.M., A.R.M., A.B., D.P. and A.C., with key input from

C. Shen, J.B., P.T., D.R., T.J. and C. Schneider. Figures were put together by J.P., M.M., A.R.M., A.C. and J.N.M. T.A.D. and S.C.J. provided KLF2–GFP mice as well as intellectual input. J.T. contributed critical advice on data analysis and visualization. Human blood samples were obtained with the help of N.G. and A.S. at the McGill University Health Center. S.C., A.E. and R.S.-N. provided key expertise throughout the project. The paper was written by J.N.M. together with J.P., M.M. and A.R.M., with contributions from all authors.

Funding

We acknowledge funding from Human Frontier Science Program Long-Term Fellowship LT000110/2019-L (to J.P.), Human Frontier Science Program grant RGP0053/2020 (to J.N.M. and J.T.), Canadian Institutes for Health Research project grant 202104PJT-462910 (to J.N.M.), Canadian Foundation for Innovation Project #32749 (to A.E.), Natural Sciences and Engineering Research Council RGPIN-2020-07169 (to A.E.) and the US National Institutes for Health, awards F31AI88630 (to T.A.D.) and R01AI38903 (to S.C.J.).

Competing interests

A.S. serves on the advisory boards, consults or is a member of the speaker bureaus for Amgen, AstraZeneca, Boehringer-Ingelheim, Bayer, Eli Lilly, HSL Therapeutics, Novo Nordisk, Novartis, Servier and Vifor Pharma. A.S. is also a co-founder and/or shareholder of Aerocardia, AREA19, FrontRx and PercAssist. The other authors declare no competing interests.

Additional information

Extended data is available for this paper at https://doi.org/10.1038/s41590-026-02581-9.

Supplementary information The online version contains supplementary material available at https://doi.org/10.1038/s41590-026-02581-9.

Correspondence and requests for materials should be addressed to Judith N. Mandl.

Peer review information *Nature Immunology* thanks Ana-Maria Lennon-Duménil and the other, anonymous, reviewer(s) for their contribution to the peer review of this work.

https://doi.org/10.1038/s41590-026-02581-9

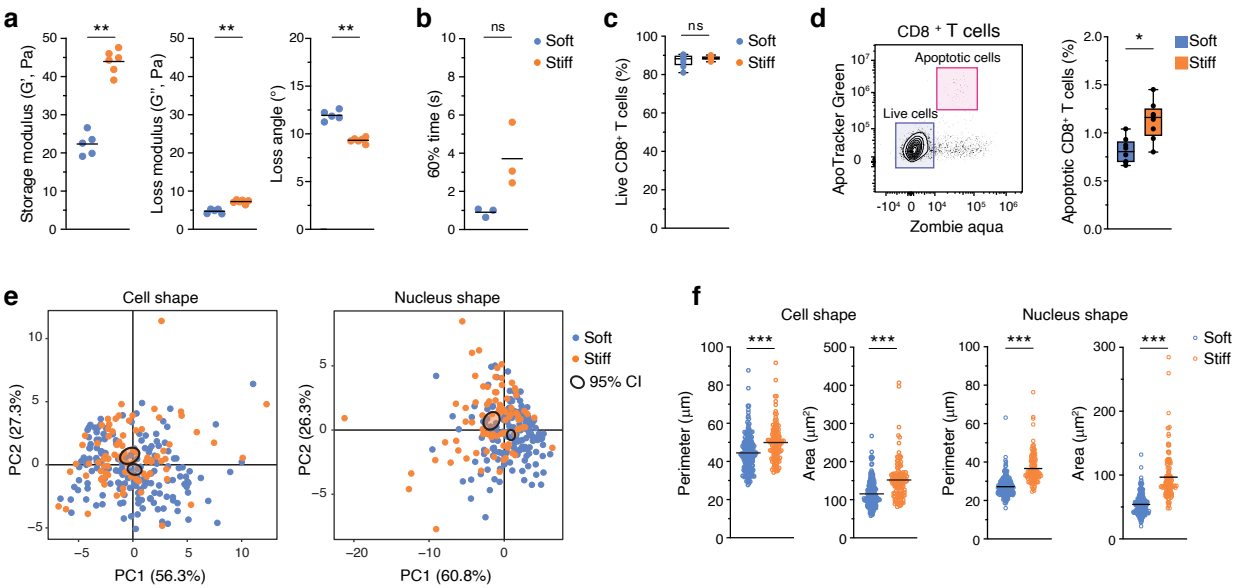

Extended Data Fig. 1 | Minimal changes in cell viability of CD8⁺ T cells in stiffer environments. a, Storage modulus (left), loss modulus (middle) and loss angle (right) of soft vs stiff collagen (n = 5-6 gels) determined by shear rheology after 15 min of an oscillatory time sweep (1% strain, 1 Hz, 37 °C isothermal gelation). **b**, Time values for relaxation to 60% of initial stress under constant deformation (20% strain) for soft vs stiff collagen (n = 3 gels). **c,d**, Percentage of live (**c**), and apoptotic (**d**) cells, of activated CD8⁺ T cells (n = 8 mice, pooled from 2 independent experiments) migrating for 24 h in soft vs stiff gels. Error bars represent median ± min/max with box boundaries denoting 25th and 75th percentiles A representative contour plot is shown in d. **e**, PCA of 20 cell and nucleus shape descriptors extracted from 2D z-projections of CD8⁺ T cells migrating for 8 h in soft (n = 162 cells) vs stiff (n = 84 cells) collagen gels (n = 3 mice). **f**, Quantification of cell and nucleus perimeter and area 24 h post-migration. Group means are shown (**a, b, c, f**). Statistical tests: Mann-Whitney (**a, b, f**); Wilcoxon (**c, d**); all statistical tests were two-sided; ns, non-significant; *P < 0.05; **P < 0.01; ***P < 0.001.

https://doi.org/10.1038/s41590-026-02581-9

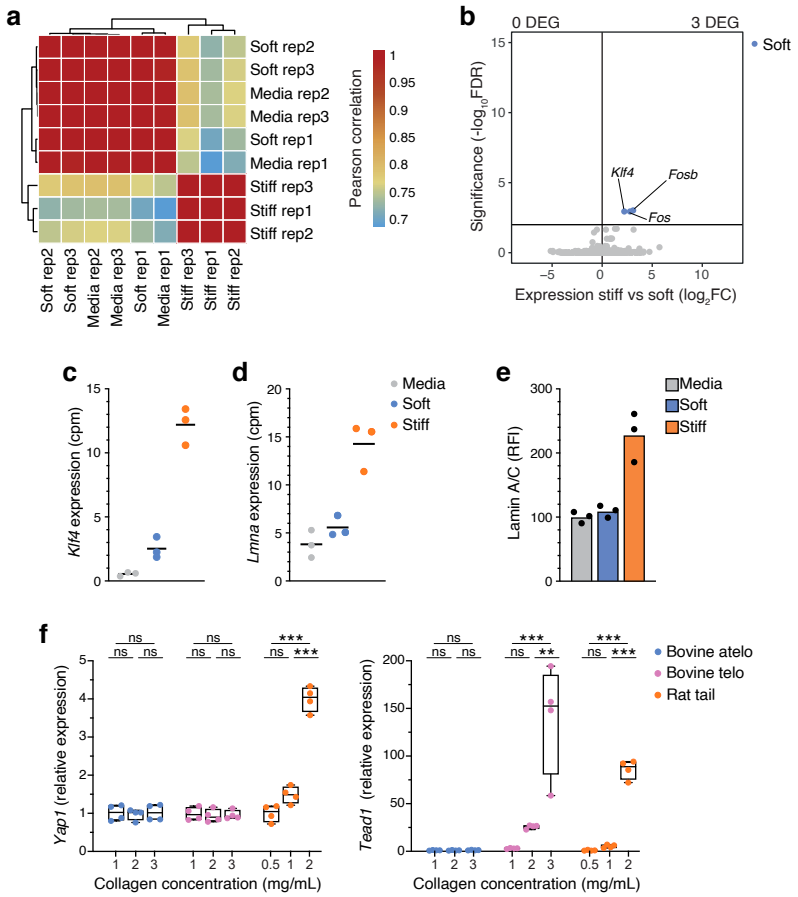

Extended Data Fig. 2 | Few transcriptional changes are detected in CD8$^+$ T cells migrating in soft collagen compared to cells in media. a,b, CPM correlation matrix (a), and volcano plot (b), of significant DEGs from RNA-seq between replicates of CD8$^+$ T cells isolated from media and soft collagen (FDR < 0.01). Positive fold change (FC) values in the volcano plot indicate increased expression in CD8$^+$ T cells in soft collagen ($n = 3$ mice). **c,d**, Expression of *Klf4* (c), and *Lmna* (d), from RNA-seq ($n = 3$ mice). **e**, Lamin A/C expression measured by flow cytometry in the same cells as used for RNA-seq ($n = 3$ mice). **f**, *Yap1* and *Tead1* gene expression (relative to housekeeping gene and normalized to the 1 mg ml^{-1} atelo-bovine condition) measured by RT-qPCR in activated CD8$^+$ T cells 24 h after embedding in 1, 2, and 3 mg ml^{-1} atelo- and telo-bovine collagen, and 0.5, 1, and 2 mg ml^{-1} telo-rat tail collagen ($n = 4$ mice, pooled from 2 independent experiments). Medians shown in all quantification plots (**c, d, e**); each data point is from an individual mouse (except for volcano plot where each data point is a gene). Error bars are median ± min/max with box boundaries denoting 25th and 75th percentiles (**f**). Statistical tests: ANOVA with Tukey's multiple comparisons test (**f**); all statistical tests were two-sided; ns, non-significant; $^{**}P < 0.01$; $^{***}P < 0.001$.

https://doi.org/10.1038/s41590-026-02581-9

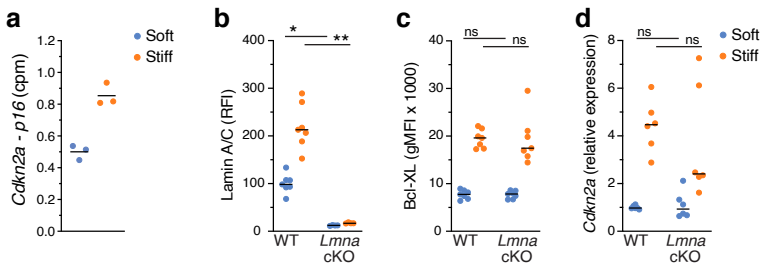

Extended Data Fig. 3 | Mechanically induced DNA damage does not increase in the absence of lamin A/C expression. a, Expression of *Cdkn2a* (p16) in RNA-seq of $CD8^+$ T cells ($n = 3$ mice) from soft vs stiff collagen gels. Lines denote means per group. **b**, Activated Vav-cre^+ $Lmna^{fl/fl}$ (*Lmna* cKO) or Vav-cre^- $Lmna^{fl/fl}$ (WT) $CD8^+$ T cells ($n = 4$ or 8 mice, pooled from 2 independent experiments) were embedded in soft or stiff collagen for 24 h and expression of lamin A/C measured by flow cytometry. **c**, Bcl-XL expression measured by flow cytometry in $CD8^+$ T cells ($n = 7$ mice, pooled from 2 independent experiments) as in a. **d**, Expression of *Cdkn2a* determined by RT-qPCR in $CD8^+$ T cells ($n = 7$ mice, pooled from 2 independent experiments) as in a. Medians shown in all quantification plots (**a**-**d**); each data point is from an individual mouse. Statistical tests: ANOVA with Dunn's multiple comparisons test (**b**,**d**); ANOVA with Šídák's correction for multiple comparisons (**c**); all statistical tests were two-sided; ns, non-significant; $^*P < 0.05$; $^{**}P < 0.01$.

https://doi.org/10.1038/s41590-026-02581-9

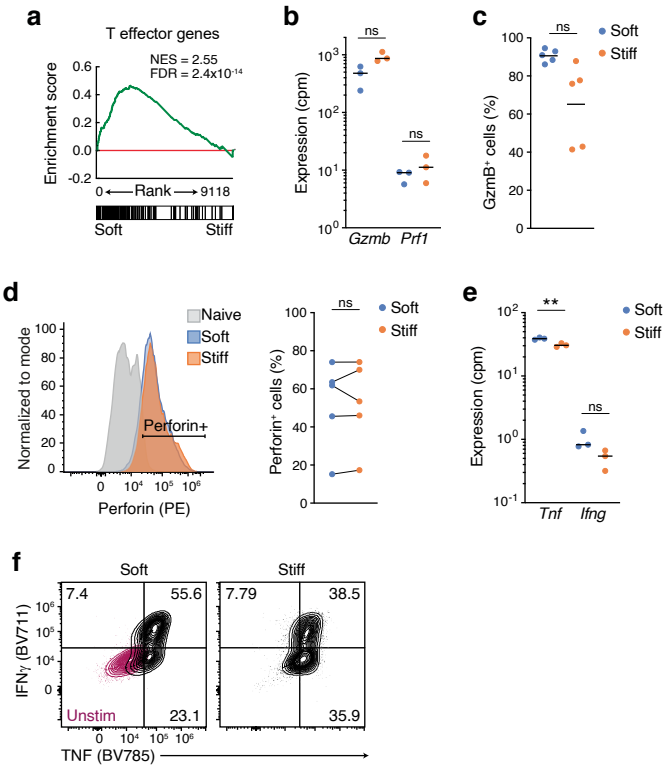

Extended Data Fig. 4 | Increased mechanical input does not impact CD8⁺ T cell effector function. a, GSEA of T effector genes (ref. 65) enriched in DEGs from RNA-seq of CD8⁺ T cells ($n = 3$ mice) migrating in soft (2 mg ml^{-1} atelo-bovine) or stiff (2 mg ml^{-1} telo-rat tail) collagen for 24 h. **b**, Expression of *Gzmb* (granzyme B) and *Prf1* (perforin) from soft vs stiff RNA-seq ($n = 3$ mice) as in a. **c**, Granzyme B expression in P14 CD8⁺ T cells activated with GP33 peptide-pulsed splenocytes ($n = 5$ mice) quantified by flow cytometry after migrating for 24 h in soft vs stiff collagen. **d**, Representative histogram and quantification of perforin expression in naive and CD3 + CD28 Ab activated CD8⁺ T cells measured by flow cytometry, migrating for 24 h in soft vs stiff collagen. **e**, Expression of *Tnf* and *Ifng* from soft vs stiff RNA-seq ($n = 3$ mice) as in a. **f**, CD3 + CD28 Ab activated CD8⁺ T cells migrating in soft vs stiff collagen for 24 h were assessed for IFNγ and TNF expression by flow cytometry either without stimulation or after PMA/ionomycin stimulation for 4 h. Medians shown in all quantification plots (**b, c, d, e**). Statistical tests: Benjamini-Hochberg method with FDR < 0.01 (**b, e**); Wilcoxon (**c, d**); all statistical tests were two-sided; ns, non-significant; $^{**}P < 0.01$; $^{***}P < 0.001$.

https://doi.org/10.1038/s41590-026-02581-9

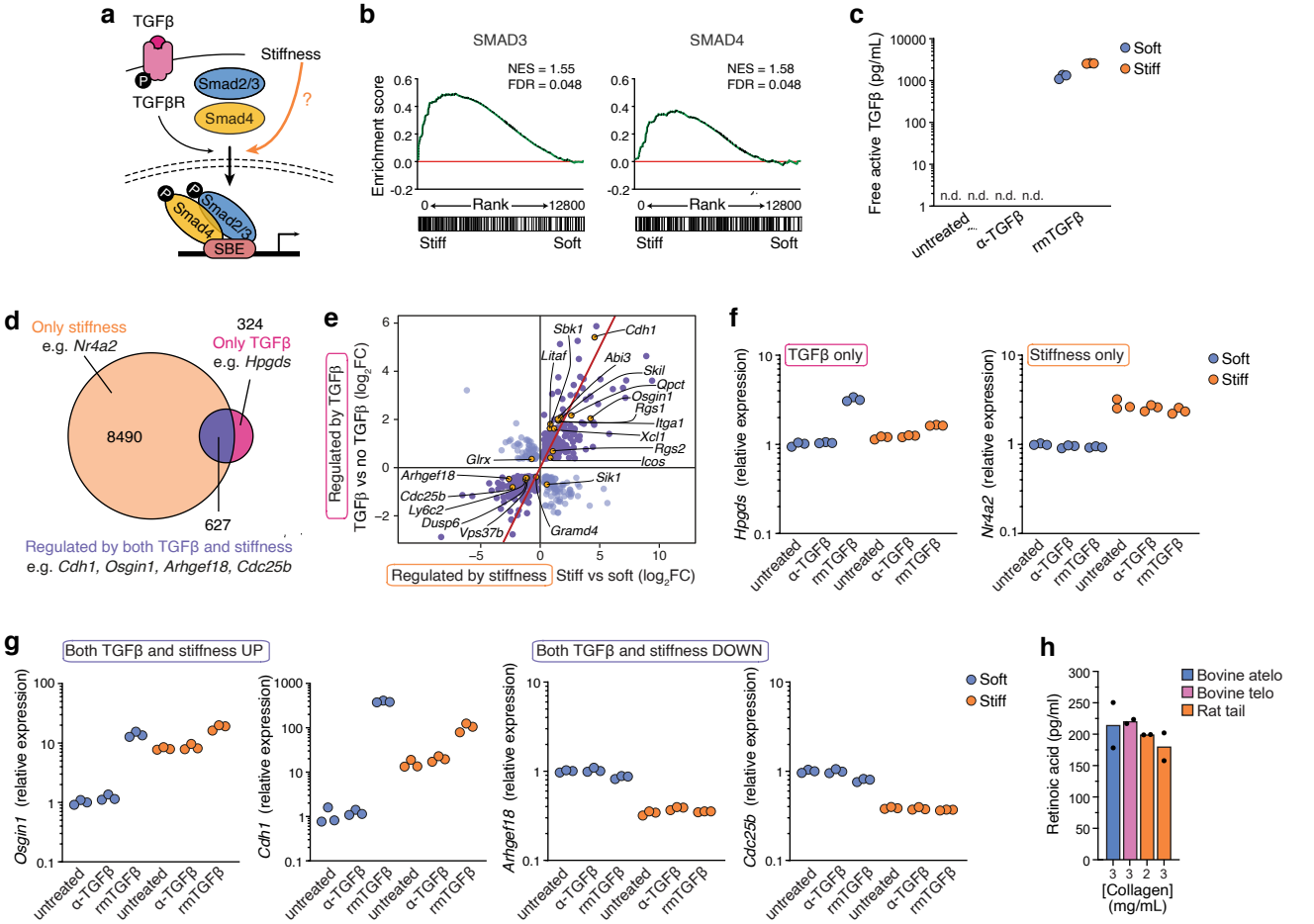

Extended Data Fig. 5 | TGFβ does not drive the mechano-induced T_{RM}-like phenotype. a, Simplified schematic of the TGFβ-receptor signaling pathway. **b**, GSEA of SMAD3 and SMAD4 signatures from MSigDB #M6325 and #M18670, respectively, enriched in genes from RNA-seq of $CD8^+$ T cells migrating in soft (2 mg ml-1 atelo-bovine) or stiff (2 mg ml-1 telo-rat tail) collagen for 24 h. **c**, Quantification of the concentration of free active TGFβ in soft vs stiff collagen gels with CD3 + CD28 Ab activated $CD8^+$ T cells ($n = 3$ mice) left untreated or treated with α-TGFβ or recombinant murine (rm) TGFβ for 24 h. Samples were defined as non-detectable (n.d.) when the absorbance was below that of the lowest standard (7.8 pg/ml). **d**, Venn diagram showing the intersection between stiffness-regulated significant DEGs identified by RNA-seq (FDR < 0.01, $n = 3$ mice) and the TGFβ-regulated genes (ref. 44). **e**, Expression fold change of the genes regulated both by stiffness and TGFβ (purple area in the Venn diagram in (**d**)). A total of 491 genes are correlated (regulated by TGFβ and stiffness in the same direction, darker purple data points) while 136 genes are anti-correlated (lighter purple data points). Red line indicates identity line. **f**,**g**, Expression of *Hpgds* and *Nr4a2* (**f**), *Osgin1, Cdh1, Arhgef18*, and *Cdc25b* (**g**), by RT-qPCR in $CD8^+$ T cells ($n = 3$ mice) migrating for 24 h in soft vs stiff gels left untreated or treated with α-TGFβ or rmTGFβ as in c. **h**, Quantification of retinoic acid by ELISA in 3 mg ml-1 atelo-bovine collagen, 3 mg ml-1 telo-bovine collagen, and 2 and 3 mg ml-1 telo-rat tail collagen. Technical replicates ($n = 2$).

https://doi.org/10.1038/s41590-026-02581-9

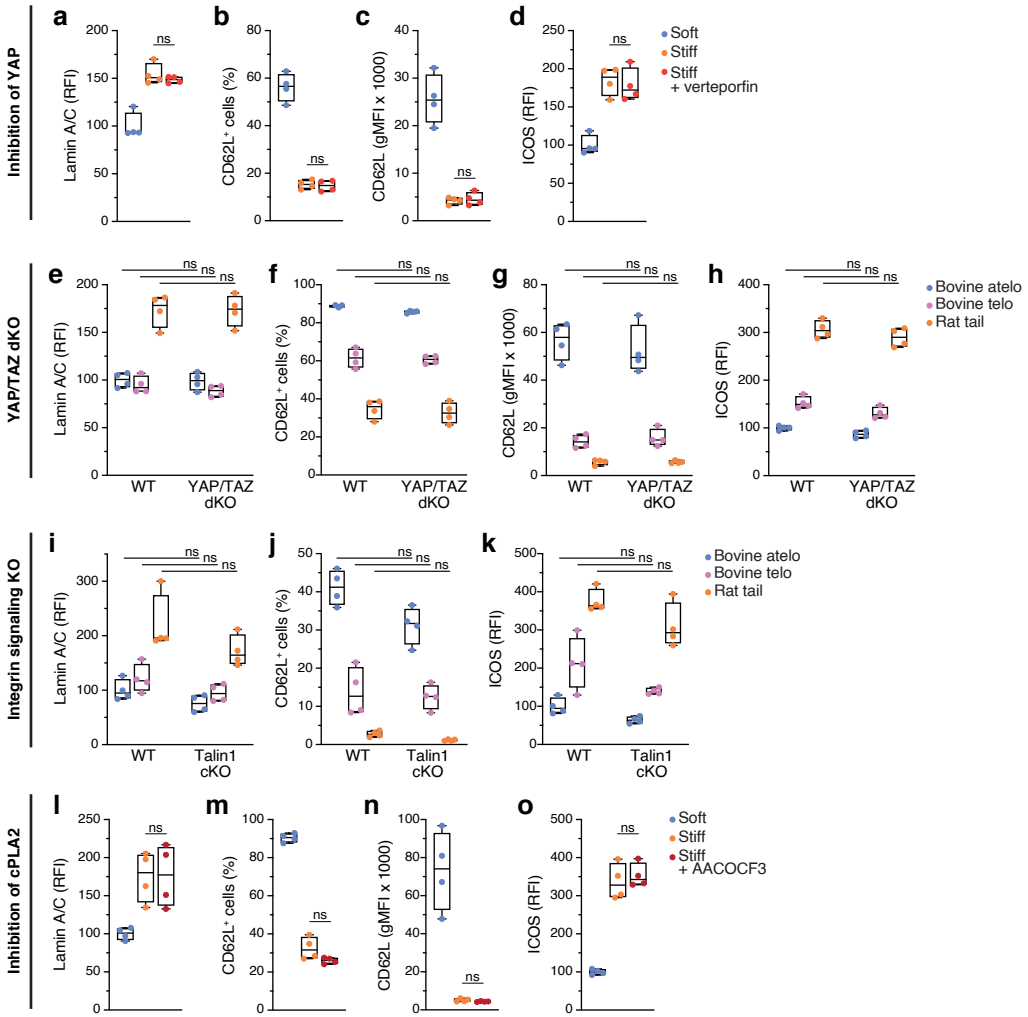

Extended Data Fig. 6 | Lamin A/C upregulation and TRM cell-like phenotype are not abrogated by Talin1- or YAP/TAZ-deficiency, or by cPLA2 inhibition. **a-d**, $CD8^+$ T cells activated with CD3 + CD28 Ab ($n = 4$ mice) were embedded in soft (2 mg ml^{-1} atelo-bovine) or stiff (2 mg ml^{-1} telo-rat tail) collagen for 24 h with or without the YAP inhibitor verteporfin, and expression of lamin A/C (a), CD62L (b,c), and ICOS (d) measured by flow cytometry. **e-h**, Tat-cre-treated $Yap1^{fl/fl}Wwtr1^{fl/fl}$ (YAP/TAZ dKO) or Tat-cre-treated $Yap1^{+/+}Wwtr1^{+/+}$ (wild-type) $CD8^+$ T cells activated with CD3 + CD28 Ab ($n = 4$ mice/genotype) were embedded in 2 mg ml^{-1} atelo-bovine, 2 mg ml^{-1} telo-bovine, or 2 mg ml^{-1} telo-rat tail collagen and expression of lamin A/C (e), CD62L (f-g), and ICOS (h) measured by flow cytometry. **i-k**, Tat-cre-treated $talin1^{fl/fl}$ (Talin cKO) or $talin1^{+/+}$ (wild-type) $CD8^+$ T cells were activated and embedded in collagen ($n = 4$ mice/genotype) as in e-h, and expression of lamin A/C (i), CD62L (j), and ICOS (k) measured by flow cytometry. **l-o**, WT $CD8^+$ T cells ($n = 4$ mice) were embedded in soft or stiff gels as in a-d, with or without the $cPLA_2$ inhibitor AACOCF3, and expression of lamin A/C (l), CD62L (m-n), and ICOS (o) measured by flow cytometry. Error bars represent median ± min/max with box boundaries denoting 25th and 75th percentiles (**a-o**); each data point is from an individual mouse; RFIs are normalized to the atelo-bovine collagen mean. Statistical tests: Wilcoxon (**a-d, l-o**); ANOVA with Dunn's multiple comparisons test (**e-k**); all statistical tests were two-sided; ns, non-significant.

https://doi.org/10.1038/s41590-026-02581-9

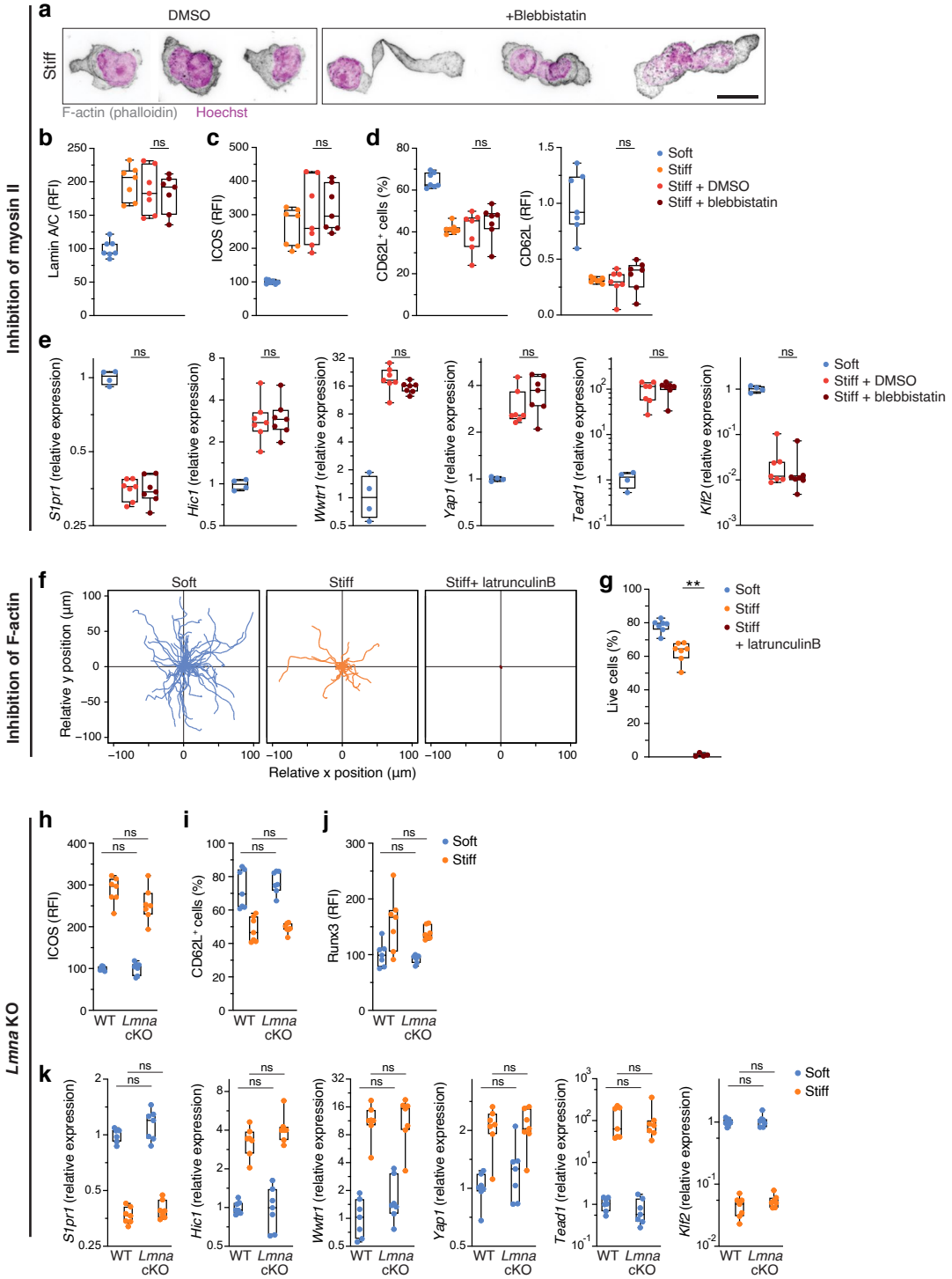

Extended Data Fig. 7 | T_{RM} cell-like phenotype is not abrogated by lamin A/C-deficiency or myosin II inhibition. a, Confocal images of DMSO- or blebbistatin-treated CD3 + CD28 Ab activated CD8$^+$ T cells migrating through stiff (2 mg ml^{-1} telo-rat tail) collagen gels for 6 h; 3 representative cell examples shown per group ($n = 3$ mice). **b-d**, CD8$^+$ T cells activated with CD3 + CD28 Ab ($n = 7$ mice, pooled from 2 independent experiments) were embedded in soft (2 mg ml^{-1} atelo-bovine) or stiff (2 mg ml^{-1} telo-rat tail) collagen for 24 h with or without the myosin II inhibitor blebbistatin, and expression of lamin A/C (**b**), ICOS (**c**), and CD62L (**d**) measured by flow cytometry, RFI normalized to the soft condition mean. **e**, Expression of *S1pr1, Hic1, Wwtr1, Yap1, Tead1*, and *Klf2* was determined by RT-qPCR in CD8$^+$ T cells ($n = 4$ or 7 mice, pooled from 2 independent experiments) as in b-d. **f**, Cell tracks from live cell microscopy data of CD8$^+$ T cells ($n = 2$ mice) activated with CD3 + CD28 Ab migrating in soft ($n = 73$ cells) vs stiff ($n = 59$ cells) collagen, or treated with latrunculin B in stiff collagen ($n = 61$ cells) for 30 min 8 h after being embedded in collagen. Cell tracks are shown from one representative experiment. **g**, CD8$^+$ T cells activated with CD3 + CD28 Ab ($n = 4$ or 7 mice, pooled from 2 independent experiments) either untreated or treated with latrunculin B as in f, and percent live cells measured after 24 h of migrating in collagen gels by flow cytometry. **h-k**, WT or *Lmna* cKO CD8$^+$ T cells were activated with CD3 + CD28 Ab ($n = 7$ mice, pooled from 2 independent experiments) and embedded in soft vs stiff collagen for 24 h. Expression of ICOS (h), CD62L (i), and Runx3 (j) was measured by flow cytometry, RFI normalized to the soft condition mean. Expression *of S1pr1, Hic1, Wwtr1, Yap1, Tead1*, and *Klf2* (k), was determined by RT-qPCR. In all quantification plots, each data point is from an individual mouse. Error bars are median ± min/max with box boundaries denoting 25th and 75th percentiles (**b-d, g-k**). Statistical tests: Mann-Whitney (**b-e, g**); ANOVA with Dunn's multiple comparisons test (**h-k**); all statistical tests were two-sided; ns, non-significant; $^{**}P < 0.01$; $^{***}P < 0.001$.

https://doi.org/10.1038/s41590-026-02581-9

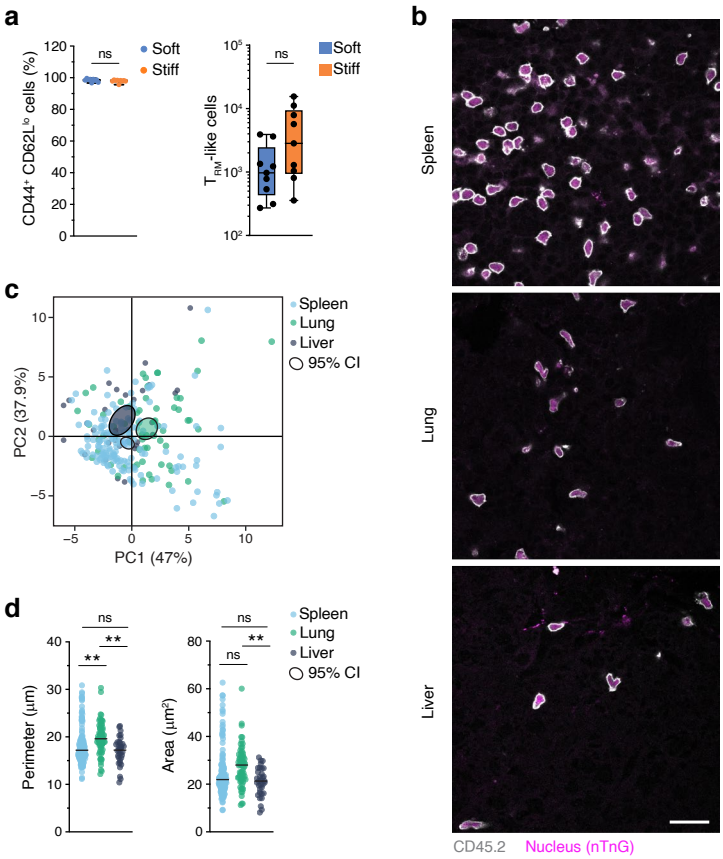

Extended Data Fig. 8 | Analysis of adoptively transferred effector CD8⁺ T cell phenotype and shape across tissues. a, Percent and number of CD62L^{lo} cells derived from the CD8⁺ T cells preconditioned in soft vs stiff collagen, adoptively transferred intradermally and then retrieved from ear pinnae ($n = 9$ mice, pooled from 2 independent experiments) 7 days post transfer. **b**, CD45.2⁺ nTnG T cells were activated with CD3 + CD28 Ab, expanded with IL-2 and on day 4 after activation adoptively transferred into CD45.1⁺ recipients infected with LCMV 4 days prior. Spleen, lung and liver were harvested 28 days post infection and imaged by confocal microscopy after staining for CD45.2. Representative z-slices are shown ($n = 2$ mice; 2 lung, 2 spleen and 2 liver sections were imaged per mouse). **c**, PCA of nuclear shape descriptors of CD45.2⁺ nTnG T cells in parenchyma of spleen ($n = 150$ nuclei), lung ($n = 64$ nuclei), and liver ($n = 33$ nuclei) from experiment in b. 95% confidence intervals (CI) of standard errors of the mean are shown for each tissue. **d**, Quantification of nucleus shape parameters across tissues as in c; data points are individual cells; medians are shown (**a, d**). Error bars are median ± min/max with box boundaries denoting 25th and 75th percentiles (**a**). Statistical tests: Mann-Whitney (**a**); ANOVA with Tukey's multiple comparisons (**d**)**;** all statistical tests were two-sided**;** ns, non-significant; $^{**}P < 0.01$.

nature portfolio

Corresponding author(s): Judith N. Mandl

Last updated by author(s): Jun 2, 2026

Reporting Summary

Nature Portfolio wishes to improve the reproducibility of the work that we publish. This form provides structure for consistency and transparency in reporting. For further information on Nature Portfolio policies, see our Editorial Policies and the Editorial Policy Checklist.

Statistics

For all statistical analyses, confirm that the following items are present in the figure legend, table legend, main text, or Methods section.

n/a	Confirmed
☐	☒ The exact sample size (*n*) for each experimental group/condition, given as a discrete number and unit of measurement
☐	☒ A statement on whether measurements were taken from distinct samples or whether the same sample was measured repeatedly
☐	☒ The statistical test(s) used AND whether they are one- or two-sided *Only common tests should be described solely by name; describe more complex techniques in the Methods section.*
☒	☐ A description of all covariates tested
☐	☒ A description of any assumptions or corrections, such as tests of normality and adjustment for multiple comparisons
☐	☒ A full description of the statistical parameters including central tendency (e.g. means) or other basic estimates (e.g. regression coefficient) AND variation (e.g. standard deviation) or associated estimates of uncertainty (e.g. confidence intervals)
☐	☒ For null hypothesis testing, the test statistic (e.g. *F*, *t*, *r*) with confidence intervals, effect sizes, degrees of freedom and *P* value noted *Give P values as exact values whenever suitable.*
☒	☐ For Bayesian analysis, information on the choice of priors and Markov chain Monte Carlo settings
☐	☒ For hierarchical and complex designs, identification of the appropriate level for tests and full reporting of outcomes
☒	☐ Estimates of effect sizes (e.g. Cohen's *d*, Pearson's *r*), indicating how they were calculated

Our web collection on statistics for biologists contains articles on many of the points above.

Software and code

Policy information about availability of computer code

Data collection	Optics11 Piuma Nanoindenter Software v3; Harmony v5.2; Zen 3.4; Leica Las X, FACSDiva v8; SpectroFlo v3.2; StepOne Software v2.2.2
Data analysis	Optics11 Piuma Nanoindenter Software v3; ImageJ Fiji v2.10.4; Imaris v10; FlowJo v10 ; GraphPad Prism v10; R Project v4.3.1; RStudio v2023.09.1; GSEA v4.3.2; celltrackR 1.2.1; cellpose v3.0

For manuscripts utilizing custom algorithms or software that are central to the research but not yet described in published literature, software must be made available to editors and reviewers. We strongly encourage code deposition in a community repository (e.g. GitHub). See the Nature Portfolio guidelines for submitting code & software for further information.

Data

Policy information about availability of data

All manuscripts must include a data availability statement. This statement should provide the following information, where applicable:

- Accession codes, unique identifiers, or web links for publicly available datasets
- A description of any restrictions on data availability
- For clinical datasets or third party data, please ensure that the statement adheres to our policy

RNA sequencing dataset can be accessed in GSE278556. All other data are available upon request from the corresponding author (J.N.M).

Research involving human participants, their data, or biological material

Policy information about studies with human participants or human data. See also policy information about sex, gender (identity/presentation), and sexual orientation and race, ethnicity and racism.

Reporting on sex and gender	Blood samples were collected from different sexes and genders, but due to low sample sizes and because this was beyond the scope of the study, sex- and gender-based analyses were not conducted.
Reporting on race, ethnicity, or other socially relevant groupings	Race, ethnicity or other socially relevant groupings were not recorded for the human samples collected, and therefore whether these variables may impact the immune parameters measured was not assessed in this study.
Population characteristics	Adult individuals were recruited for this study at random from the pool of researchers at McGill University. Individuals sampled had no ongoing or current symptoms of infection and were not on any immuno-suppressive medication. Individuals were aged 21 - 45 yrs old and thus whether responses differ in the elderly was not assessed in this study.
Recruitment	see above.
Ethics oversight	This study was approved by the McGill University Health Center Research Ethics Board (human ethics protocol #2023-8829).

Note that full information on the approval of the study protocol must also be provided in the manuscript.

Field-specific reporting

Please select the one below that is the best fit for your research. If you are not sure, read the appropriate sections before making your selection.

☒ Life sciences ☐ Behavioural & social sciences ☐ Ecological, evolutionary & environmental sciences

For a reference copy of the document with all sections, see nature.com/documents/nr-reporting-summary-flat.pdf

Life sciences study design

All studies must disclose on these points even when the disclosure is negative.

Sample size	Sample size was determined based on prior in vivo work in our laboratory to allow us to identify differences between groups, perform reliable statistical analyses, and ensure reproducibility.
Data exclusions	For flow cytometry experiments using cells isolated from tissues, samples were excluded in case of a FACS clog during the acquisition or if the number of recovered transferred cells was below 50.
Replication	Where possible, all experiments were repeated three times, independently. The number of times each experiment was independently repeated is indicated in figure legends.
Randomization	Animals were randomly assigned to study groups within each genotype. Mice were age- and sex-matched and littermate controls were used where possible.
Blinding	Image analyses were automated to avoid the introduction of bias. All other analyses were performed unblinded, as in our study mice or cells were grouped by genotype and/or treatment rather than subjective allocation.

Reporting for specific materials, systems and methods

We require information from authors about some types of materials, experimental systems and methods used in many studies. Here, indicate whether each material, system or method listed is relevant to your study. If you are not sure if a list item applies to your research, read the appropriate section before selecting a response.

Materials & experimental systems

n/a	Involved in the study
☐	☒ Antibodies
☒	☐ Eukaryotic cell lines
☒	☐ Palaeontology and archaeology
☐	☒ Animals and other organisms
☒	☐ Clinical data
☒	☐ Dual use research of concern
☒	☐ Plants

Methods

n/a	Involved in the study
☒	☐ ChIP-seq
☐	☒ Flow cytometry
☒	☐ MRI-based neuroimaging

Antibodies

Antibodies used

All antibodies and other reagents used are listed in supplementary table 4.

Bcl-xL (54H6) Rabbit mAb (PE-Cy7® Conjugate); clone: 54H6; source: Cell Signaling Technology; Cat#: 81965S; RRID: AB_2936839
Brilliant Violet 421™ anti-mouse CD8a Antibody; clone: 53-6.7; source: BioLegend; Cat#: 100738; RRID: AB_11204079
BD Horizon™ RB780 Rat Anti-Mouse CD8a; clone: 53-6.7; source: BD Biosciences; Cat#: 568692; RRID: AB_2936840
PE/Fire™ 700 anti-mouse CD8a Antibody; clone: 53-6.7; source: BioLegend; Cat#: 100792; RRID: AB_2876397
BD Horizon™ BUV395 Mouse Anti-Human CD8; clone: RPA-T8; source: BD Biosciences; Cat#: 563795; RRID: AB_2722501
BD Horizon™ BB700 Rat Anti-Mouse CD44; clone: IM7; source: BD Biosciences; Cat#: 566506; RRID: AB_2744396
Brilliant Violet 650™ anti-mouse CD45.2 Antibody; clone: 104; source: BioLegend; Cat#: 109836; RRID: AB_2563065
BV785 rat anti-mouse CD62L; clone: MEL-14; source: BioLegend; Cat#: 104440; RRID: AB_2629685
PE/Cyanine7 anti-mouse CD69 Antibody; clone: H1.2F3; source: BioLegend; Cat#: 104512; RRID: AB_493565
Brilliant Violet 421™ anti-mouse CD103 Antibody; clone: 2E7; source: BioLegend; Cat#: 121422; RRID: AB_2562901
TruStain FcX (anti-mouse CD16/32); clone: 93; source: BioLegend; Cat#: 101302; RRID: AB_312801
Human TruStain FcX (Fc Receptor Blocking Solution); clone: -; source: BioLegend; Cat#: 422302; RRID: AB_2818986
PE/Cyanine7 anti-mouse CD278 (ICOS) Antibody; clone: 7E.17G9; source: BioLegend; Cat#: 117421; RRID: AB_2860636
Lamin A/C (4C11) Mouse mAb (Alexa Fluor® 488 Conjugate); clone: 4C11; source: Cell Signaling Technology; Cat#: 8617S; RRID: AB_10997529
Phospho-Chk1 (Ser345) (133D3) Rabbit mAb (PE Conjugate); clone: 133D3; source: Cell Signaling Technology; Cat#: 12268S; RRID: AB_2797863
BD Pharmingen™ PE Mouse Anti-RUNX3; clone: R3-5G4; source: BD Biosciences; Cat#: 564814; RRID: AB_2738969
Brilliant Violet 605™ anti-mouse CD90.1 (Thy-1.1) Antibody; clone: OX-7; source: BioLegend; Cat#: 202537; RRID: AB_2562644
Phospho-Histone H2A.X (Ser139) Antibody, PerCP-eFluor™ 710; clone: CR55T33; source: eBioscience; Cat#: 46-9865-42; RRID: AB_2573918
CD4 Monoclonal Antibody (GK1.5), eFluor 450, eBioscience; clone: GK1.5; source: ThermoFisher; Cat#: 48-0041-82; RRID: AB_10718983
Lamin A/C (4C11) Mouse Monoclonal Antibody (Alexa Fluor 647 Conjugate); clone: 4C11; source: Cell Signaling Technology; Cat#: 41357S; RRID: Submitted
BD Horizon™ BUV395 Rat Anti-Mouse CD44; clone: IM7; source: ThermoFisher; Cat#: 363-0441-82; RRID: AB_2925262
Alexa Fluor 647 anti-human/mouse Granzyme B Antibody; clone: GB11; source: BioLegend; Cat#: 515405; RRID: AB_2294995
PE anti-mouse Perforin; clone: S16009A; source: BioLegend; Cat#: 154305; RRID: AB_2721638
Brilliant Violet 711™ anti-mouse IFN-gamma Antibody; clone: XMG1.2; source: BioLegend; Cat#: 505836; RRID: AB_2650928
Brilliant Violet 785™ anti-mouse TNF-alpha; clone: MP6-XT22; source: BioLegend; Cat#: 506341; RRID: AB_2565951
alpha Tubulin Monoclonal Antibody (B-5-1-2), Alexa Fluor 488; clone: B-5-1-2; source: Invitrogen; Cat#: 322588; RRID: AB_2532182
CD45.2 Monoclonal Antibody (104), Alexa Fluor 647; clone: 104; source: Invitrogen; Cat#: A14737; RRID: AB_2534253
CD31 (PECAM-1) (D8V9E) Rabbit Monoclonal Antibody; clone: D8V9E; source: Cell Signaling Technology; Cat#: 77699S; RRID: AB_2722705
Goat anti-Rabbit IgG (H+L) Cross-Adsorbed Secondary Antibody, Alexa Fluor 514; clone: -; source: Invitrogen; Cat#: A-31558; RRID: AB_2536173

Validation

All antibodies are commercially available and have been validated by the manufacturers/suppliers.

Animals and other research organisms

Policy information about studies involving animals; ARRIVE guidelines recommended for reporting animal research, and Sex and Gender in Research

Laboratory animals

C57BL/6J (jax #000664), B6.Thy1.1 (jax #000406), B6.CD45.1 (jax #033076), and vav-cre (jax #03567056) mice were purchased from The Jackson Laboratory. LifeAct-GFP reporter mice57 (shared by J. Burkhardt, University of Pennsylvania) were crossed in-house with nTnG reporter mice (jax #02353758). YAPfl/fl/TAZfl/fl mice59 were shared by A. Gregorieff (McGill); Thy1.1+ P14 TCR transgenic mice60 by H. Melichar (McGill). Lmnafl/fl mice61 were shared by J. Lammerding (Cornell University) and crossed to vav-cre mice in-house. All mice were bred and housed under SPF conditions in the CMARC animal facility (McGill), in accordance with the Guide for the Care and Use of Laboratory Animals, with exception of KLF2-GFP reporter (51) mice, which were bred at the University of Minnesota in the lab of S. Jameson and spleens shipped on ice to Montreal. All mice were on a C57BL/6J background and used for experiments at 6-12 weeks of age. Both male and female mice were used and sex-matched where applicable. Randomization and blinding were not used. The sample size was determined by power analysis and prior experience. No datapoints were excluded from the analyses. Experimental procedures were all approved by the McGill University Facility Animal Care Committee (protocol #MCGL-7570). Mice were housed in a 12h/12h light/dark cycle at an ambient temperature of 18-24 degrees Celsius and a humidity range of 30-70%.

Wild animals

No wild animals were used in this study.

Reporting on sex

Data was analysed for possible sex-effects and pooled if there were no differences between male and female mice.

Field-collected samples

No field-collected samples were used in this study.

Ethics oversight

All animal studies were approved by the McGill University Facility Animal Care Committee (protocol #MCGL-7570)

Note that full information on the approval of the study protocol must also be provided in the manuscript.

Plants

Seed stocks	N/A
Novel plant genotypes	N/A
Authentication	N/A

Flow Cytometry

Plots

Confirm that:

☒ The axis labels state the marker and fluorochrome used (e.g. CD4-FITC).

☒ The axis scales are clearly visible. Include numbers along axes only for bottom left plot of group (a 'group' is an analysis of identical markers).

☒ All plots are contour plots with outliers or pseudocolor plots.

☒ A numerical value for number of cells or percentage (with statistics) is provided.

Methodology

Sample preparation	Staining: 2×10^6 cells per condition were distributed in wells of a 96-well V-bottom plate. Less cells were used when rarer populations were stained, for instance when isolating TRM cell-like cells. In a dark place, extracellular staining of cells was performed using a combination of fluorescently conjugated monoclonal antibodies diluted in FACS buffer supplemented with a viability dye and either TruStain FcX (anti-mouse CD16/32 antibody, BioLegend) or Human TruStain FcX (Fc Receptor Blocking Solution, BioLegend) for 20 min at 4°C. Samples requiring intracellular staining were washed in PBS before being fixed using 2% PFA for 30 min at 4°C. Cells were washed using FACS buffer before performing the intracellular staining with a combination of fluorescently conjugated monoclonal antibodies diluted in FACS buffer supplemented with 0.3% Triton X-100 and TruStain FcX for 60 min at 4°C. Cells were washed in FACS buffer and resuspended in 200 µL ice-cold FACS buffer. Samples were filtered over a 60 µm nylon mesh and kept on ice until analysis using a flow cytometer. The fluorescently conjugated monoclonal antibodies used are listed above and in Supplementary Table 4.
Instrument	Acquisition: Samples were acquired on a LSRFortessa flow analyzer (BD Biosciences) or a Aurora spectral flow analyzer (Cytek).
Software	Data were analyzed with FlowJo software v10 (BD Biosciences).
Cell population abundance	n/a
Gating strategy	For all experiments: Cells selected by FSC/SCC. Doublets removed by FSC-A/FSC-W gate and SSC-A/SSC-W gate. Dead cells excluded with viability dye. Gating strategy for TRM cells provided in Figure 5. Raw data examples are provided throughout manuscript.

☐ Tick this box to confirm that a figure exemplifying the gating strategy is provided in the Supplementary Information.